Wave prediction by means of two distinct approaches: Numerical modelling and deep-learning

波浪予測の二つの方法、数値モデルと深層学習の検討

June 2021

Thit Oo KYAW
チョー テイツー ウー

Wave prediction by means of two distinct approaches: Numerical modelling and deep-learning

波浪予測の二つの方法、数値モデルと深層学習の検討

June 2021

Waseda University
Graduate School of Creative Science and Engineering
Department of Civil and Environmental Engineering,
Research on Coastal Engineering and Management

Thit Oo KYAW
チョー テイツー ウー

Acknowledgements

First and foremost, the author would like to specially thank to her academic supervisor, Professor Tomoya SHIBAYAMA for his continuous support and helpful suggestions throughout the research period. Without his proper guidance and inspiration, this research would not have been successful and complete the doctoral program.

The author also feels thankful to Prof. Miguel Esteban and Dr. Martin Maell for sharing their knowledge in every aspect and for their precious support towards publishing the research work internationally. The author acknowledges every member of Shibayama Laboratory for their kind help on academic matters and for creating a comfortable social life while studying together.

The author is sincerely grateful to Waseda University for providing the Special Scholarship, which was a great financial support to study in Japan for five years. The author expresses her heartfelt thanks to her family and friends for their endless support and encouragement. Lastly, the author thanks every single person who helps from all sides contributing to the successful completion of this research.

Abstract

The accurate prediction of wave characteristics and parameters is of the utmost importance for coastal planning and construction projects. Over the years, wave prediction has mainly been conducted by means of empirical formulations and numerical simulations. Most recently, machine learning based wave forecasting models have become popular as cutting-edge wave prediction techniques. In the present thesis, two different wave prediction methodologies were developed. The first one includes the estimations of the time-series of extreme wave parameters due to cyclones by using existing numerical models. The second one involves the prediction of near-real-time wave conditions by developing a new machine-learning based wave forecasting model.

For the first case methodology, the Weather Research and Forecasting (WRF) and Simulating WAves Nearshore (SWAN) models were applied in a top-down numerical simulation approach. The wind output of WRF was subsequently used as an input to SWAN, from which the significant wave height (H_s), peak wave period (T_p) and peak wave direction were obtained. As a case study, this WRF-SWAN model was used to hindcast the extreme wave characteristics caused by cyclone Nargis at Myanmar coast. The model results were compared with observed data from Indian Meteorological Department (IMD), National Oceanic and Atmospheric Administration (NOAA) as well as with the satellite measured wave data. Since Myanmar lacks a dense network of in-situ wave observation stations, the study results suggest the potential and reliable usage of numerical wave modelling along with the satellite altimetry wave records for applications in coastal areas in countries like Myanmar.

For the latter case of conditional wave forecasting, a deep-learning based wave forecasting model was developed to classify the wave conditions (either low or high).

Specifically, the Long Short Term Memory (LSTM) neural network, which is a kind of Recurrent Neural Network (RNN) was used. The training, testing and validation of the model were conducted by using the in-situ wave data (from the Nationwide Ocean Wave information network for Ports and HArbourS; NOWPHAS) at various locations along the Japan coast. The model was run to forecast the next 24 h of wave conditions (high or low) based on the previous 24 h, 48 h and 72 h wave data. The results show that the overall average wave classification accuracy of the model ranges from around 75 % to 99 % (with accuracies above 98% if at least three years of data are used to train the model). Since the accurate prediction of low wave conditions is essential for planning of offshore construction work, the model can be used as a practical tool to reduce the potential waste of resources in such projects.

In summary, the present research concerns with two different methods of wave prediction; the traditional numerical wave modelling and the advanced deep-learning approach. Each methodology highlights the different potential usage and applications of available measured wave data (ranging from satellite and in-situ wave stations). Based on the present study, it can be concluded that the numerical modelling technique is essentially applicable for exceptional extreme wave conditions, while the cutting-edge deep learning approach can be more effective for the prediction of seasonal waves in order to conduct real-time operational planning at coastal areas.

Table of Contents

List of Figures

List of Tables

List of Abbreviations

AFWA	Air Force Weather Agency
ANN	Artificial Neural Network
ARW	Advanced Research WRF
BOB	Bay of Bengal
BODC	British Oceanographic Data Centre
CD	Coupled Discrete
CH	Coupled Hybrid
CNES	Centre National d'Études Spatiales
DMH	Department of Meteorology and Hydrology
DP	Decoupled Propagation
ENVISAT	ENVironmental SATellite
ERS	European Remote Sensing
ESA	European Space Agency
FAA	Federal Aviation Administration
FFNN	Feed Forward Neural Network
FN	False Negatives
FNL	Final
FP	False Positives
FSL	Forecast Systems Laboratory
GDAS	Global Data Assimilation System
GEBCO	General Bathymetric Chart of the Oceans
GEOSAT	GEOdetic SATellite
GFO	Geosat Follow-On
GFS	Global Forecast System
IMD	India Meteorological Department
JASON	Joint Altimetry Satellite Oceanography Network
LSTM	Long Short Term Memory
NASA	National Aeronautics and Space Administration
NCAR	National Center for Atmospheric Research
NCEP	National Centers for Environmental Prediction
NGDC	National Geophysical Data Centre
NMM	Non-hydrostatic Mesoscale Model
NOAA	National Oceanic and Atmospheric Administration

NOWPHAS	Nationwide Ocean Wave information network for Ports and HArbourS
RNN	Recurrent Neural Network
RSMC	Regional Specialized Meteorological Center
SWAMP	Sea WAve Modeling Project
TC	Tropical Cyclone
TN	True Negatives
TP	True Positives
USGS	U.S. Geological Survey
WAM	WAve Modeling
SWAN	Simulating WAves Nearshore
WPS	WRF Pre-processing System
WRF	Weather Research and Forecasting
WW3	WaveWatch 3

List of Parameters

η	terrain-following hydrostatic-pressure vertical coordinate
p	pressure
p_h	hydrostatic component of the pressure
p_{hs}	hydrostatic pressure along the surface
p_{ht}	hydrostatic pressure along the top boundaries
μ	hydrostatic pressure difference between surface and top boundaries
Ω	contravariant vertical velocity
t	time
u	horizontal component of velocity in x-direction
v	horizontal component of velocity in y-direction
w	vertical component of velocity
ϕ	geopotential
θ	potential temperature, wave direction
g	gravitational acceleration
F_U	Forcing term from model physics
F_v	Forcing term from turbulent mixing
F_w	Forcing term from spherical projections
F_Θ	Forcing term from earth's rotation
x, y, z	east, north, and vertical axes in the Cartesian coordinate system
u, v, w	x, y, z velocity components
N	action density spectrum
σ	wave relative frequency
λ	longitude
φ	latitude
H_s	Significant wave height
T_s	Significant wave period
S_{in}	wind-wave interaction
S_{ds}	dissipation of wave energy
S_{nl}	non-linear wave-wave interactions
W_s	wind speed
W_{dir}	wind direction

1 Introduction

1.1 Background

The accurate prediction of wave characteristics is essential for coastal planning and construction projects. The history of wave prediction goes back to the1940s, starting with the development of the first empirical formulations for this purpose (Sverdrup et al. 1947), followed by the development of first, second and third generation numerical wave models (Mandal & Prabaharan, 2010). Over the years, wave prediction has mainly conducted by traditional numerical simulations, as their reliability has generally been improving (Booij et al., 1999; Samiksha et al., 2015). Most recently, machine learning based wave forecasting models have been developed as a cutting-edge wave prediction technique, and their integrated usage with physics-based numerical wave model has become popular (O'Donncha et al. 2018).

Generally, the occurrence of extreme waves can have a high influence on the design and planning coastal infrastructure, including port development and maintenance, the operation of offshore structures or coastal protection. Near-real-time wave forecasting is essential for nearshore and offshore construction and maintenance projects, as the accurate prediction of when low waves will take place is also essential to decide whether work will proceed or not. Therefore, it is imperative to analyse and select an appropriate wave prediction method depending on the purpose of the application such as whether to calculate the design parameters of coastal structures or to plan out the working schedule of offshore construction site. In addition, the availability and accessibility of observed wave data at a given area can also affect the selection of suitable wave prediction techniques for initiating and planning of coastal projects.

Given this, in the present thesis different wave prediction schemes were developed by means of two comparative approaches using numerical models and artificial neural networks. The first one is the time-series prediction (hindcasting) of extreme wave parameters due to cyclones by means of numerical modelling, using Myanmar as the case study area, given the lack of available in-situ wave data records. The second one is the prediction of near-real-time wave conditions by developing a new machine-learning based wave forecasting model, which was applied to the case of the Japanese coast, given its dense wave buoy observation network (with data available for several decades), which makes it possible to apply the machine learning with artificial neural networks.

1.2 Literature Review

1.2.1 Numerical Wave Models

Since 1960s, many numerical wave models were developed with their types being differed according to the consideration of energy source functions, water depth at application area (shallow or deep water) and the numerical procedures and physical equations for solving the energy transport process. Among them, the consideration of nonlinear energy transfer of waves in the space (S_{nl}) mainly defines the type of the wave model. Therefore, based on the different S_{nl} terms in the numerical wave models, they can be distinguished into three main types, which are i) Decoupled Propagation (DP) models, ii) Coupled Hybrid (CH) models and iii) Coupled Discrete (CD) models. From 1960s to 1970s, DP models were developed, and they are known as first-generation wave models. Later from the 1970s to 1980s, CH and CD models were developed and they are classified as second-generation wave models.

By the mid-80s, although the first- and second-generation wave models were operational to a certain extent, in order to compare the physics of the various models and to

assess their strengths and weaknesses, a major international intercomparison study was initiated; the Sea WAve Modelling Project, SWAMP, (SWAMP Group, 1985). As a first step to improve the above-mentioned wave models, Klaus Hasselmann invited wave researchers to Hamburg to discuss the possibility of a joint endeavor in the spring of 1984 and then the WAM (WAve Modelling) group was formed in 1988. The aim of the group was to develop a third-generation model, free from many of the assumptions which constrained earlier generation models. Variants of this basic model were also developed by Tolman (1991) (WAVEWATCH) and more recently by Booij et al (1996), which resulted in the Simulating WAves Nearshore (SWAN) model. In order to outperform the first- and second-generation models, this third-generation wave model takes into accounts the followings:

i. Wave propagation in time and space, shoaling, refraction due to current and depth, frequency shifting due to currents and non-stationary depth

ii. Wave generation by wind

iii. Three and four-wave interactions

iv. White-capping, bottom friction, and depth-induced breaking

v. Wave-induced setup

vi. Propagation from laboratory up to global scales

vii. Transmission through and reflection from obstacles

Generally, for hindcasting of ocean waves, the numerical wave models are widely used in a consolidated modelling network to provide reanalysis of ocean wave data in globally and regionally gridded domains. They are also currently applied for near real time forecasting of wind-generated waves, with the wind forcing obtained from different

meteorological sources such as in-situ data and remote sensing. For calibration of simulated wave parameters, the corresponding simulated wave data are validated against the observed global wave data network, which is made up of in-situ wave measurement stations and (James et al. 2018).

1.2.2 Neural Networks in Wave Modelling

Over the years, given the development and application of machine learning in different areas of study, their potential usefulness in coastal engineering has also increased. Long-term recorded wave data, which is available from established global wave observation buoy networks as well that recorded by vessels, allows the use of Artificial Neural Networks (ANNs) for wave modelling. The applicability of ANNs ranges from wave hindcasting and forecasting to the study of non-linear wave properties and interactions with coastal structures in both shallow and deep water, as long as reliable data is available.

In contrast to physics-based numerical wave models, which require various types of high resolution input datasets such as bathymetry and wind data , ANNs possess the ability to recognize the relationship between inputs and outputs rather than the physical phenomenon (Mandal and Paraban, 2010). With the ability to learn the hidden structure in the datasets, the ANNs can directly estimate the targeted results without calling for additional physical datasets (Schmidhuber 2015; LeCun 2015; Goodfellow et al. 2016). Since an ANN wave model can be obtained by training, testing and validating based on the known inputs-outputs, it is potentially applicable to cases where the physical phenomena is ambiguous and computationally expensive to be executed by numerical wave models (DeVries et al. 2017).

In terms of recent studies of wave prediction using ANNs, Londhe et al. (2016) proposed an ANN based error prediction method (univariate time-series forecasting) between

forecasted and observed wave heights at Indian coastline. Kumar et al. (2017) used sequential learning network and an ensemble of Extreme Learning Machine (Ens-ELM) to predict the daily wave heights. James et al. (2017) applied a multi-layer perceptron (MLP) conceptual model of supervised machine learning for wave prediction. Shrivastava and Chaturvedi (2018) used a direct acting (feed-forward) neural network with correlation of wave parameters at five NOAA buoys in Caribbean Sea. In general, these studies mainly conducted a time-series wave parameter prediction using feed-forward neural networks as an application of ANNs in coastal and offshore engineering.

1.3 Objectives and Scope of Work

The present research concerns itself with two different methods of wave prediction: a traditional numerical wave modelling approach and another more advanced deep-learning approach. The main objective of the research is to highlight the different types of usage of these two wave prediction techniques, based on their purpose of application and the availability of locally observed wave data. The work can thus be subdivided into two objectives, which highlight how different methods can be used at the two extremes of data availability. Essentially, Objective 1 will regard the development of a methodology that can hindcast waves when very little wave observation data is available, while Objective 2 will explain how advanced techniques can be used to provide accurate forecasting when a wealth of observation data is available.

1.3.1 Objective 1: Hindcasting of Extreme Waves Induced by Cyclones with Little Observational Data

In order to showcase how the hindcasting of extreme waves induced by cyclone can be done when little observational data is available, the present thesis will investigate the case of Nargis at the coast of Myanmar. For that, a numerical simulation approach using the Weather Research and Forecasting (WRF) and Simulating WAves Nearshore (SWAN) models was conducted to study the meteorological and offshore wave characteristics of this cyclone. The wind output of WRF was subsequently used as input to SWAN, from which simulated values of significant wave height (H_s), peak wave period (T_p) and peak wave direction were obtained. The WRF simulation results agree well with the observed data from the India Meteorological Department. SWAN simulation results were compared with the WaveWatch 3 model by National Oceanic and Atmospheric Administration and validated against available measurement data from satellites.

1.3.2 Objective 2: Wave Forecasting using Advanced Deep-learning Approaches

A deep-learning based wave forecasting model was developed to classify wave conditions (either low or high) in areas where a wealth of wave observational data exists. Specifically, the Long Short Term Memory (LSTM) neural network, which is a kind of Recurrent Neural Network (RNN), was utilized. The model was applied at Tottori and Kashima along the Japanese coast. The training, testing and validation of the model were conducted by using the in-situ wave data (from the Nationwide Ocean Wave information network for Ports and HArbourS; NOWPHAS) at various locations along the Japan coast. The model was run for different preceding times and forecasted wave classification results (low or high waves) up to 24 h in the future were provided.

2 Numerical Simulations of Extreme Waves Induced by Cyclone Nargis at Myanmar Coast

2.1 Introduction

Coastal environments are often exposed to high waves and surges caused by storms, which can result in severe socio-economic impacts. Understanding the extreme wave conditions that can take place during cyclonic events is essential for designing and planning coastal infrastructure, including port development and maintenance, the operation of offshore structures or coastal protection. Myanmar is a country that is frequently affected by Tropical Cyclones (TCs) originating from the Bay of Bengal (BOB), where the first seasonal storms usually develop during the pre-monsoon period (April or May), and the second round of TCs occurs during the post-monsoon period (around October or November). During the monsoon, the enhanced vertical wind shear produced by the prevailing south-westerlies (in lower) and easterlies (in upper troposphere) inhibits the development of TCs (Tasnim et al., 2015b; Fosu and Wang, 2015). Thus, between June to September, tropical disturbances over the BOB are mostly limited to monsoon depressions (Yoon and Huang, 2012). In general, cyclone tracks do not veer towards Myanmar, and therefore the country is less exposed to cyclonic events compared to other countries in the BOB basin (such as Bangladesh, see Tasnim et al., 2015a). However, a number of authors have claimed that, in the late 20th century, the TCs that have formed over the BOB have not only become more intensified during their lifetime (Singh et al., 2001), but also that an increasing number of them have had an impact to Myanmar due to the deepened monsoon trough (Hoarau et al., 2012; Wang et al., 2013).

TC Nargis developed over the BOB during the pre-monsoon season in late April and early May 2008 and went on to become the most devastating storm in the recorded history of Myanmar. It made landfall on the Ayeyarwady deltaic coast on 2 May 2008 as a category

four cyclone on the Saffir-Simpson scale (Lin et al., 2009). At the point of landfall, it generated a storm surge greater than 5 m, with a maximum recorded water level of 7 m at Pyinsalu, as reported by Myanmar's Department of Meteorology and Hydrology (DMH). Also, from the field survey conducted by Shibayama et al. (2009, 2010), a maximum storm surge of 4.33 m was reported near the Yangon river. The cyclone affected 50 townships along the deltaic coast, including Yangon, the largest city and former capital of Myanmar. Nargis caused over 85,000 deaths, with around 54,000 people still missing, and a 25% loss in the annual rice production of the entire country. The total damage to the infrastructure, social and productive sectors was estimated to be over 4 billion USD (Baker et al., 2008).

Much research has been conducted on the impact assessment of cyclone Nargis and disaster risk management (Baker et al., 2008; UNEP, 2009). Several numerical studies have also been conducted in an attempt to reproduce cyclone Nargis and its storm surge. A hindcast of the event, based on a sensitivity analysis of physical parameters of the WRF model, was performed by Raju et al. (2011), whereas Srinivas and Bhaskar Rao (2014) studied the role of vortex initialization in the WRF model for reproducing the storm. Nayak et al. (2012) simulated the nearshore wave induced setup along the India's Kalpakkam coast during the passage of cyclone Nargis. Simulations of cyclone Nargis's weather field and its associated storm surge were also conducted by Saito et al. (2010).

Specifically, Tasnim et al. (2015b) conducted a hypothetical study on the effects of global warming on the cyclogenesis of Nargis and how this might affect future storm surges. However, no recent studies have focused on the development and analysis of extreme offshore waves due to this cyclone, which is an important information for planning any future on- and offshore projects. Therefore, the present study highlights the estimation of the wave parameters near the Myanmar coast due to cyclone Nargis, which can support the design and planning of coastal infrastructure in the area. Essentially, it is feared that as a consequence of

global warming, the intensity of tropical cyclones could increase worldwide (Emanuel, 2005; Tsuboki, 2008; Knutson et al., 2010; Nakamura et al., 2016), increasing the risks involved in the construction of coastal infrastructure.

Given such problems, it is clearly important to improve the understanding of how tropical cyclones currently affect coastlines, and the wave fields that can be generated as a result. However, up to date relatively little research has been conducted on the characteristics of the offshore winds and waves that are possible in the vicinity of Myanmar coast during the passage of a cyclone. Part of the reason for this lack of research resides in technological constraints, such as an insufficient number of offshore official data stations and a lack of available records. Although there are wave modelling frameworks that provide ocean wave data at a global scale such as National Oceanic and Atmospheric Administration (NOAA), the available wave data has limitations due to the coarse temporal and spatial resolutions. Thus, in the present study the author attempt to simulate cyclone Nargis and its offshore wind waves by using the Weather Research and Forecasting (WRF) and Simulating WAves Nearshore (SWAN) models at a regional scale (in contrast to earlier studies, which focused mostly on the storm surge along the coast).

The reliability and performance of the applied numerical models (WRF and SWAN) will also be analysed. For this, the WRF simulated TC Nargis parameters will be compared with the observed data from the India Meteorological Department (IMD). Furthermore, the wave results from SWAN will be compared with wave data provided by NOAA. Also, they will be validated with satellite altimetry wave data, with the aim of observing the reliability of SWAN and the possible applicability of satellite measured waves at areas like Myanmar coast, where a limited historical wave data records are available.

2.2 Study Area and Cyclone Nargis

The Republic of the Union of Myanmar is situated in Southeast Asia. It is bounded by a 1,930 km long contiguous coastline, connecting to the Andaman Sea to the south and the BOB to the west. The litoral area of the country is characterized by having the Arakan Mountains close to the northwestern coast, the low-lying lands of the Ayeyarwady and Yangon deltas in the middle part, and the high terrains of Bilauktaung (Tenasserim Range) to the south. The detailed topography of the country and its surrounding area is shown in Figure 2.1. The total population of Myanmar is estimated to be 54 million, with more than 5 million living in low-lying coastal areas that are less than 5 m above mean sea level (MIMU, 2019). Being situated near the Equator, Myanmar possesses a tropical to subtropical monsoon climate which is characterized by three main seasons, i) the hot season from mid-February to mid-May, ii) the rainy season from mid-May to October and iii) the cold season from November to mid-February reported by CFE-DM (2017).

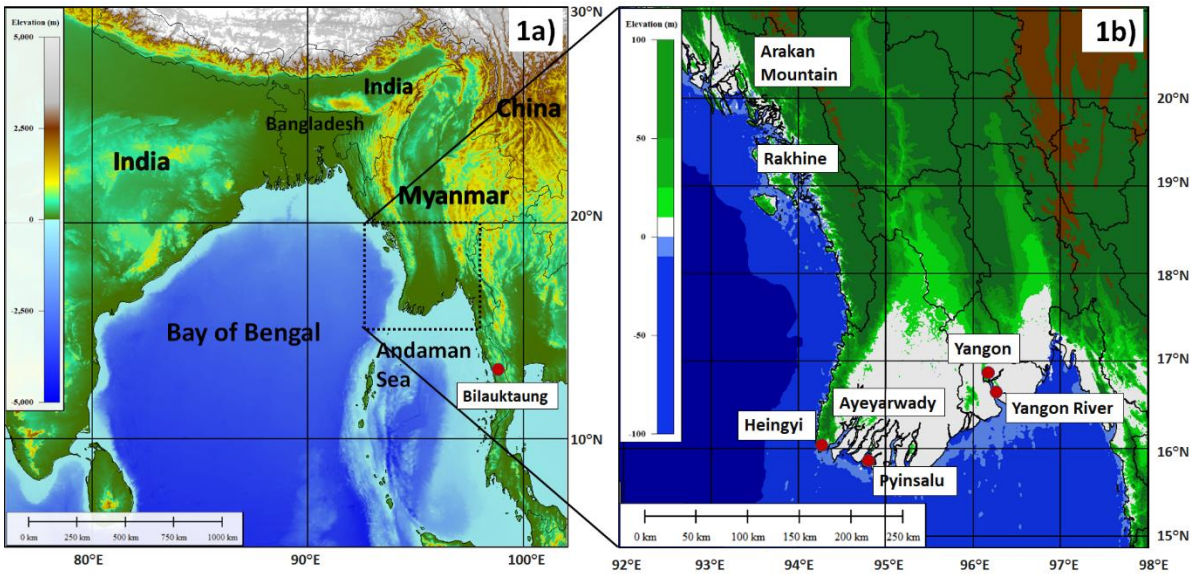

Figure 2.1 Map of Myanmar and its surrounding area, showing Rakhine coast and Ayeyarwady and Yangon deltas in detail (Elevation data from GEBCO 2020); white areas in left figure show elevation values higher than 5000 m, and in right figure low-lying regions

In the BOB basin, the earliest arrival time of the South Asian Summer Monsoon is in May (Fosu and Wang, 2015). During this time, due to the combination of monsoon trough formation, seasonally high sea surface temperatures (SST), high mid-tropospheric humidity and low vertical wind shear, there is a high tendency for TCs development (Vishnu et al., 2016). According to Myanmar's DMH, between 1887 and 2005, 80 out of the 1,248 tropical cyclones (only 6.4%) that developed over the BOB made landfall in Myanmar (the annual average number of TCs formed at BOB is 10). List of the most severe cyclones that have affected Myanmar since 1950 reported by JICA (2015) are shown in Table 2.1. Among them, only two cyclones, Pathein (1975) and Nargis (2008), made landfall at the Ayeyarwady deltaic coast, while the rest hit the western Rakhine coast of the country (see Figure 2.1). The recorded track of the cyclone Nargis and its landfall location at Ayeyarwady deltaic coast is shown in Figure 2.2.

Tropical cyclone Nargis made landfall at the Ayeyarwady delta between 2 and 3 May of 2008. The storm started as a normal monsoon depression at the center of the BOB on 27 April 2008 (see Figure 2.2). The Regional Specialized Meteorological Center (RSMC) for the Indian Ocean under the IMD stated that it reached a minimum central pressure of 962 hPa and maximum sustained surface wind speed of 47 m/s on 2 May 2008, just before making landfall at Labutta Township. The minimum hourly atmospheric pressure value archived at the inland weather stations (based on DMH data) in Yangon (Kaba Aye and Mingaladon) was approximately 974 hPa at around 23 UTC 2 May 2008.

Table 2.1 List of the most severe historical cyclones that have affected Myanmar since 1950 (Note that there is no damage data for TCs 2, 3 and 5)

No	Name	Date	Peak Surge (m)	Landfall Point	Death toll	Damage (million USD)
1.	Sittwe	7/5/1968	4.25	Sittwe	1037	2.5
2.	Pathein	7/5/1975	3.00	Pathein	304	No data
3.	Gwa	4/5/1982	3.70	Gwa	31	No data
4.	Maungdaw	2/5/1994	3.66	Maungdaw	10	10
5.	Mala	29/4/2006	4.57	Gwa	37	No data
6	Nargis	2-3/5/2008	7.01	Heingyi	138,000	4000
7.	Giri	22/10/2010	3.7	Kyaukphyu	2157	57

An interesting characteristic of Nargis was its unusual track directed towards the low-lying deltaic coast, as during the monsoon period cyclones that form over the BOB usually make landfall at the northern and northeastern coast of this area (Pattanaik and Rama Rao, 2009). More detailed information about the life cycle of Nargis can be found in Li et al. (2012) and Tasnim et al. (2015b). The extent of damage caused by Nargis can be clearly seen in satellite images of the topography of the Ayeyarwady deltaic coast before and after the passage of Nargis, where a large portion of the coastline was washed off (see Figure 2.3). The debris that resulted from the cyclone is also shown in Figure 2.4.

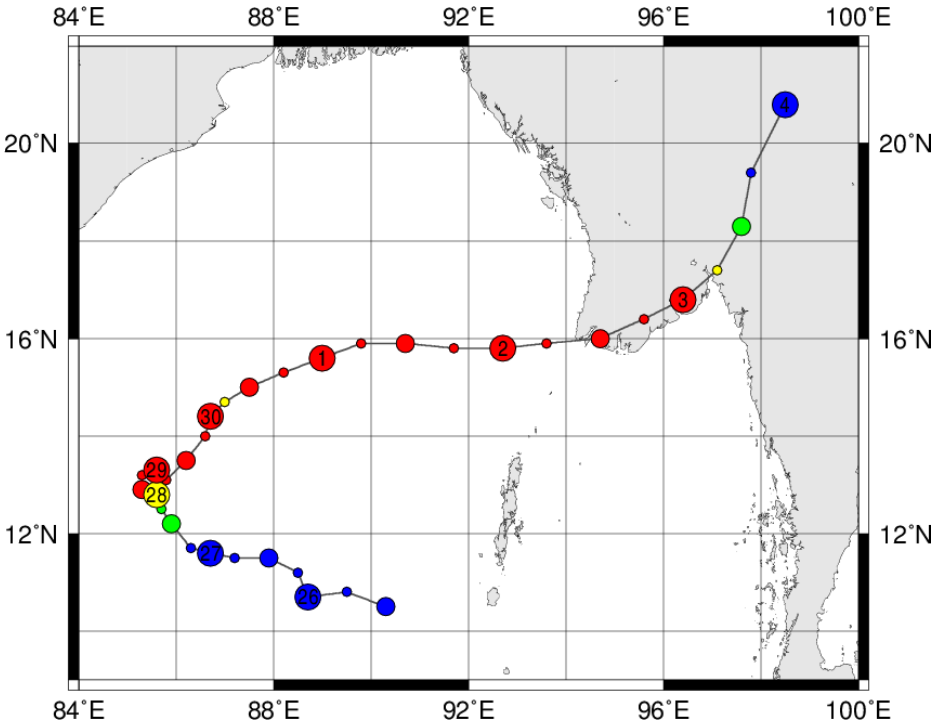

Figure 2.2 Track of Nargis from 26th April to 4th May, 2008 (Source: Digital Typhoon)

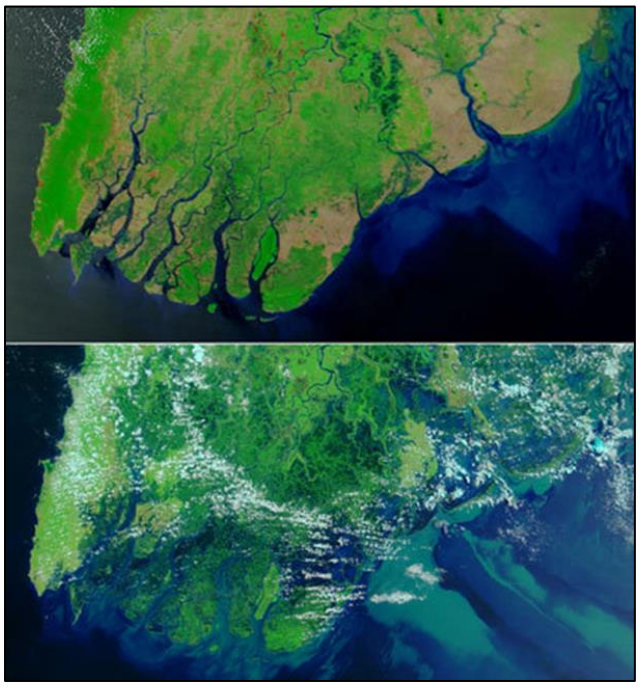

Figure 2.3 Satellite images showing the Ayeyarwady deltaic coast, Myanmar, on 15 April 2008 (top) and on 5 May 2008 (bottom) before and after Nargis made landfall (Source: NASA)

Figure 2.4 Debris due to cyclone Nargis found at Letkegon, near Yangon (Shibayama et al. 2009)

On 22 February 2018, the lead author (from Waseda University) conducted a focused group discussion with local residents of the Ayeyarwady Division to ascertain their behaviour during the event (see Figure 2.5). To organize the meeting, the lead author visited the Rural Area Developmental Project Management Training operated by the Ministry of Agriculture, Livestock and Irrigation, Myanmar. In total, there were 12 participants, all of whom were the survivors of cyclone Nargis. Participants reported how they failed to take proper precautions about the storm (despite the continuous warnings from authorities), as they had never experienced any significant storm surge event in their lifetime.

Figure 2.5 Focus group discussion regarding the behavior of local residents during the passage of cyclone Nargis

Moreover, the initial incoming surges were mistaken as normal tides, though they continued to increase. For a prolonged period of time the surge gradually rose to 2-3 m, then reaching up to 7 m when offshore waves were integrated into the surge. Hence, in the case of cyclone Nargis, the absence of public awareness about the risk of a possibility of a storm surge taking place, the lack of storm surge shelters, the occurrence of destructively strong winds and simultaneously rising surge all contributed to the substantial casualty levels that were recorded. In this respect, it is worth noting how this lack of awareness was not an uncommon issue among the Asian countries at the time. For instance, similar problems were reported for the case of typhoon Haiyan in the Philippines (Leelawat et al., 2014; Esteban et al., 2015).

2.3 Method: Numerical Modelling Framework

The modelling system for the atmospheric and wave simulations used in this study employed a top-down approach, where the output from the first model was used as an input for the next model. The general simulation framework for weather modelling and wave modelling is shown in Figure 2.6, which is similar to that used by Nishizaki et al. (2017) and Kyaw and Shibayama (2018). The first modelling step involved using Advanced version of the Weather Research and Forecasting (WRF-ARW, Skamarock et al., 2008) model. WRF is a community model, which can be implemented for both atmospheric research and operational predictions. It has a wide variety of physics and numeric options that can simulate both actual atmospheric conditions based on real observations, and idealized conditions according to NCAR (2017).

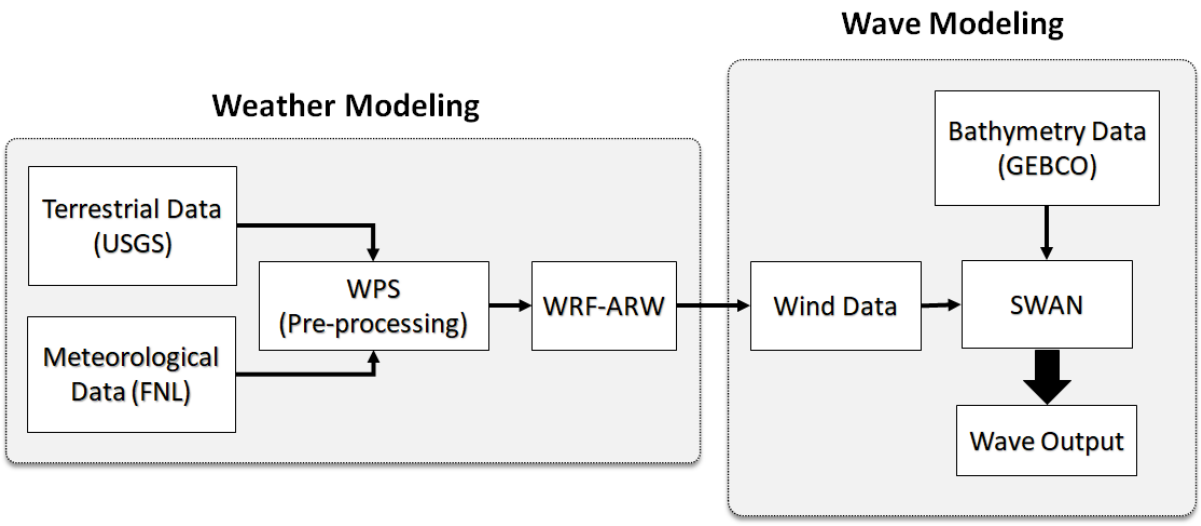

Figure 2.6 Flow chart of the models used

The second step used the third-generation wave model, Simulating WAves Nearshore (SWAN), developed at TU Delft (Booij et al., 1999). SWAN model computes random, short-

crested wind-generated waves using wave energy flux to determine their generation, propagation and dissipation in coastal regions and inland waters. The model describes the wave energy in a two-dimensional energy spectrum, as a function of wave frequency and wave direction (SWAN, 2009).

The WRF model was run first to hindcast the cyclonic wind field by setting up realistic atmospheric forcing and topographical data. Specifically, at the first stage the NCEP FNL (Final) Operational Global Analysis meteorological dataset and the U.S. Geological Survey (USGS) topographical data were used as inputs. FNL data has a 1 degree resolution that includes 27 meteorological variables, and is obtained through the Global Data Assimilation System (GDAS). The FNL meteorological grids were interpolated over the USGS geographical grids through the WRF Pre-processing System (WPS) using a Mercator map projection with a true latitude value of 30 degrees.

After these preliminary integration and interpolation steps were conducted through WPS, the gridded simulation domain for WRF was produced. Then, the weather simulation by WRF-ARW was conducted by using different physics parameterization and numeric options to achieve the best-fit parameters combination scheme for the area of interest (i.e. the BOB). Subsequently, the WRF simulated the hourly wind field output, which was extracted and then imported into the SWAN model as a wind forcing. The bathymetry data for wave simulation by the SWAN model was acquired from the General Bathymetric Chart of the Oceans (GEBCO), under the British Oceanographic Data Centre (BODC), which has a 30 arc-second resolution.

2.3.1 The WRF Model

The WRF model is a mesoscale numerical weather prediction model. The first step for the development of WRF model started in late 1990's as a collaborative work between the National Center for Atmospheric Research (NCAR), the National Oceanic and Atmospheric Administration (represented by the National Centers for Environmental Prediction (NCEP) and the (then) Forecast Systems Laboratory (FSL)), the (then) Air Force Weather Agency (AFWA), the Naval Research Laboratory, the University of Oklahoma, and the Federal Aviation Administration (FAA). WRF is a community model, currently used for both various private and public organizations worldwide such as operational weather analysis and predictions at NCEP, other national meteorological centres and in real-time forecasting configurations at laboratories, universities, and private companies. Statically, WRF has formed a large worldwide user's community over 39,000 in over 160 countries.

WRF can be applied for both atmospheric research and operational forecasting purposes. It consists of two dynamics solvers, a data assimilation system, and a parallel computing software architecture with system extensibility. It can execute a wide range of meteorological simulations from scales of tens of meters to thousands of kilometres. The two built-in dynamics cores that comprise WRF are the Advanced Research WRF (ARW) core developed at NCAR and the Non-hydrostatic Mesoscale Model (NMM) core developed at NCEP (Skamarock et al., 2008). For research purpose, WRF has a wide variety of physics and numeric options (which allow sensitivity simulation approach) that can simulate both actual atmospheric conditions based on real observations and analysis and idealized conditions on a computationally efficient platform.

2.3.1.1 The WPS and WRF Scheme

The step by step program flow of WPS and WRF is depicted in Figure 2.7. In the preliminary stage, before running the WRF, the WRF Pre-processing System (WPS) is first initiated to prepare a batch of input files with meteorological and geographical information to be executed by WRF. Calculation parameters such as boundary conditions, grid resolution, start and end date, and atmospheric physics parameterizations are controlled by each respective name list file in WPS and WRF.

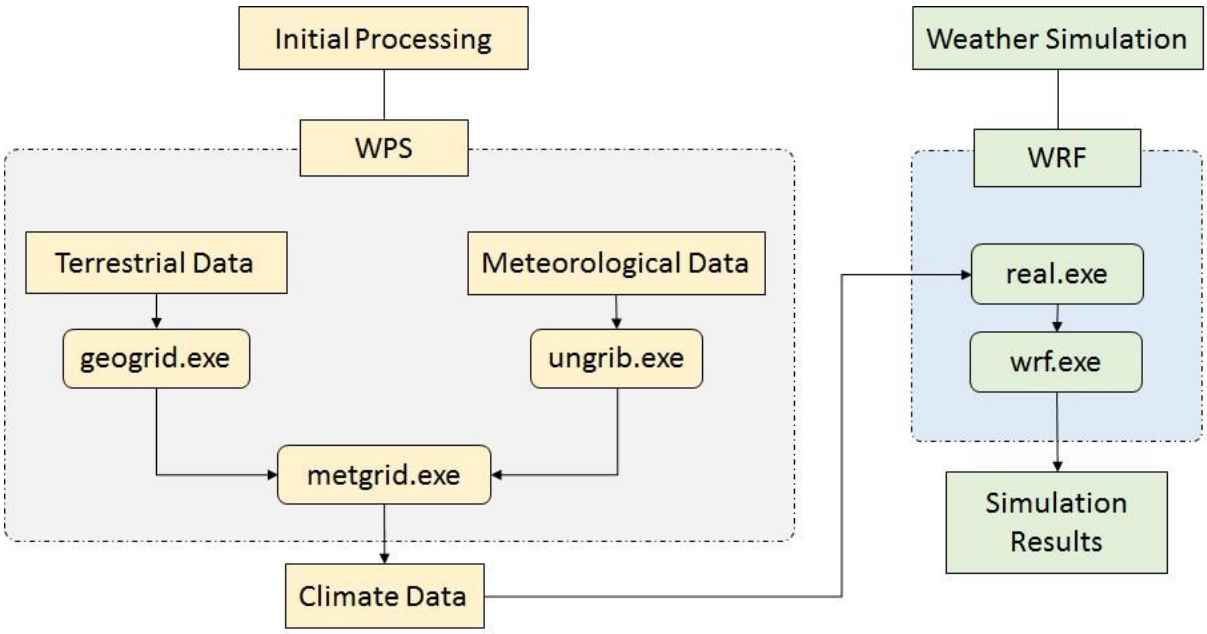

Figure 2.7 The initial WPS and WRF configuration

The WPS is composed of three main sub-programs for real data interpolation. These are (i) geogrid.exe for map projection and topographic information, (ii) ungrib.exe for information of horizontal wind, temperature, geopotential height, and relative humidity, and (iii) metgrid.exe for temporal and spatial integration of geogrid and ungrib information. The vertical interpolation of metgrid files from WPS is conducted by using the real.exe program

in WRF and, finally, wrf.exe program executes the numerical integration calculation and outputs the meteorological simulation results. The major physics options in WRF are microphysics, cumulus parametrization, planetary boundary layer, and radiation and they influence the simulation results.

2.3.1.2 Governing Equations

The governing equations of WRF are the non-hydrostatic and compressible flux form Euler equations that are solved in the dynamics core of WRF. The equations are composed of variables with conservative properties that are developed in a terrain-following mass vertical coordinate of atmospheric layers. As an extension, the effect of atmospheric moisture, spherical map projections, Coriolis and curvature terms are also included (Skamarock et al., 2008).

Firstly, the equations of the terrain-following hydrostatic-pressure vertical coordinate, η, is defined as follows;

$$\eta = (p_h - p_{ht})/\mu \tag{2.1}$$

$$\mu = p_{hs} - p_{ht} \tag{2.2}$$

where,

p_h = hydrostatic component of the pressure

p_{hs} = hydrostatic pressure along the surface

p_{ht} = hydrostatic pressure along the top boundaries

μ = hydrostatic pressure difference between surface and top boundaries

Inside the model domain, η equals to 1 at the surface and 0 at the top boundary. Then, the variables for flux form equation in terms of μ can be defined as follows;

$$V = \mu v = (U, V, W), \Omega = \mu\dot{\eta}, \Theta = \mu\theta \tag{2.3}$$

v = (u,v,w) refers to the covariant velocities in the 3 directions (2 horizontal and 1 vertical directions) while Ω is the contravariant vertical velocity, and θ is the potential temperature.

Based on the variables specified above, the Flux-Form Euler Equations in the Cartesian coordinates, neglecting the Coriolis effects, can be formulated as:

$$\frac{\partial U}{\partial t} + (\nabla \cdot V_u) - \frac{\partial}{\partial x}\left(p\frac{\partial \phi}{\partial \eta}\right) + \frac{\partial}{\partial \eta}\left(p\frac{\partial \phi}{\partial x}\right) = F_U \tag{2.4}$$

$$\frac{\partial V}{\partial t} + (\nabla \cdot V_v) - \frac{\partial}{\partial y}\left(p\frac{\partial \phi}{\partial \eta}\right) + \frac{\partial}{\partial \eta}\left(p\frac{\partial \phi}{\partial y}\right) = F_v \tag{2.5}$$

$$\frac{\partial W}{\partial t} + (\nabla \cdot V_w) - g\left(\frac{\partial p}{\partial \eta} - \mu\right) = F_w \tag{2.6}$$

$$\frac{\partial \Theta}{\partial t} + (\nabla \cdot V_\theta) = F_\Theta \tag{2.7}$$

$$\frac{\partial \boldsymbol{\mu}}{\partial t} + (\nabla \cdot V) = 0 \tag{2.8}$$

$$\frac{\partial \phi}{\partial t} + \mu^{-1}[(V \cdot \nabla \phi) - gW] = 0 \tag{2.9}$$

where,

F_U = Forcing term from model physics

F_v = Forcing term from turbulent mixing

F_w = Forcing term from spherical projections

F_Θ = Forcing term from Earth's rotation

The above equations are the descriptions of the major equations that are considered in the WRF dynamics solver. The governing equations are modified by means of perturbation to minimize the truncation errors of horizontal pressure gradient in the discrete solver and

machine rounding errors of vertical pressure gradient and buoyancy calculations. More detailed explanations of them can be accessed at the NCAR technical note of Advanced Research WRF (Skamarock et al., 2008).

2.3.2 The SWAN Model

The Simulating WAves Nearshore (SWAN) is a third-generation wave model that computes random, short-crested wind-generated waves in deep and shallow water areas. SWAN gives realistic estimates of wave parameters in coastal areas, lakes, and estuaries from given wind, bottom, and current conditions. It can be applied on grids ranging from kilometers down to a few meters and on rectangular or curvilinear grids.

Specifically, SWAN determines the wave energy flux to execute the generation, propagation and dissipation of waves in coastal regions and inland waters. The model describes the wave energy as a two-dimensional energy spectrum, as a function of the wave frequency (T^{-1}) [Hz] and the wave direction θ [°]. The SWAN model uses elliptical equations because the water particles move in elliptical orbits when the water is shallower than the wave base, which is the depth at which a surface wave can move in water.

2.3.2.1 Governing Equations

The governing equation of SWAN is configured by the spectral action balance equation. In SWAN, there are two types of spectral coordinates that are mainly differed by the type of the application domain (small-scale or large-scale). For regional small-scale domain, Cartesian coordinates are utilized whereas for global large-scale domain, Spherical coordinates are used. The spectral action balance equation formulated in terms of Spherical coordinates is as follows:

$$\frac{\partial}{\partial t}N + \frac{\partial}{\partial \lambda}c_\lambda N + (\cos\varphi)^{-1}\frac{\partial}{\partial \varphi}c_\varphi \cos\varphi N + \frac{\partial}{\partial \sigma}c_\sigma N + \frac{\partial}{\partial \theta}c_\theta N = \frac{S}{\sigma} \quad (2.10)$$

where,

N = action density spectrum = (energy density spectrum)/(relative frequency)

σ = relative frequency of wave

θ = wave direction

λ = longitude

φ = latitude

The energy density source term on the right-hand side of Equation (10) is composed of wave generation in the space, wave energy dissipation and non-linear interactions. On the left-hand side, the first, second, third, fourth and fifth terms correspond to the local rate of change of action density spectrum, propagation wave action in geo-spherical space (c_λ and c_φ in horizontal longitude and vertical latitude), the relative frequency shifting due to alternations in water depth and currents (c_θ in θ-space) and depth and current-induced refraction, respectively. The consideration of input data into the Energy Balance Equation to calculate the output wave parameters is illustrated in Figure 2.8.

$$S = S_{in} + S_{ds} + S_{nl} \quad (2.11)$$

where,

S_{in} = wind-wave interaction

S_{ds} = dissipation of wave energy

S_{nl} = non-linear wave-wave interactions

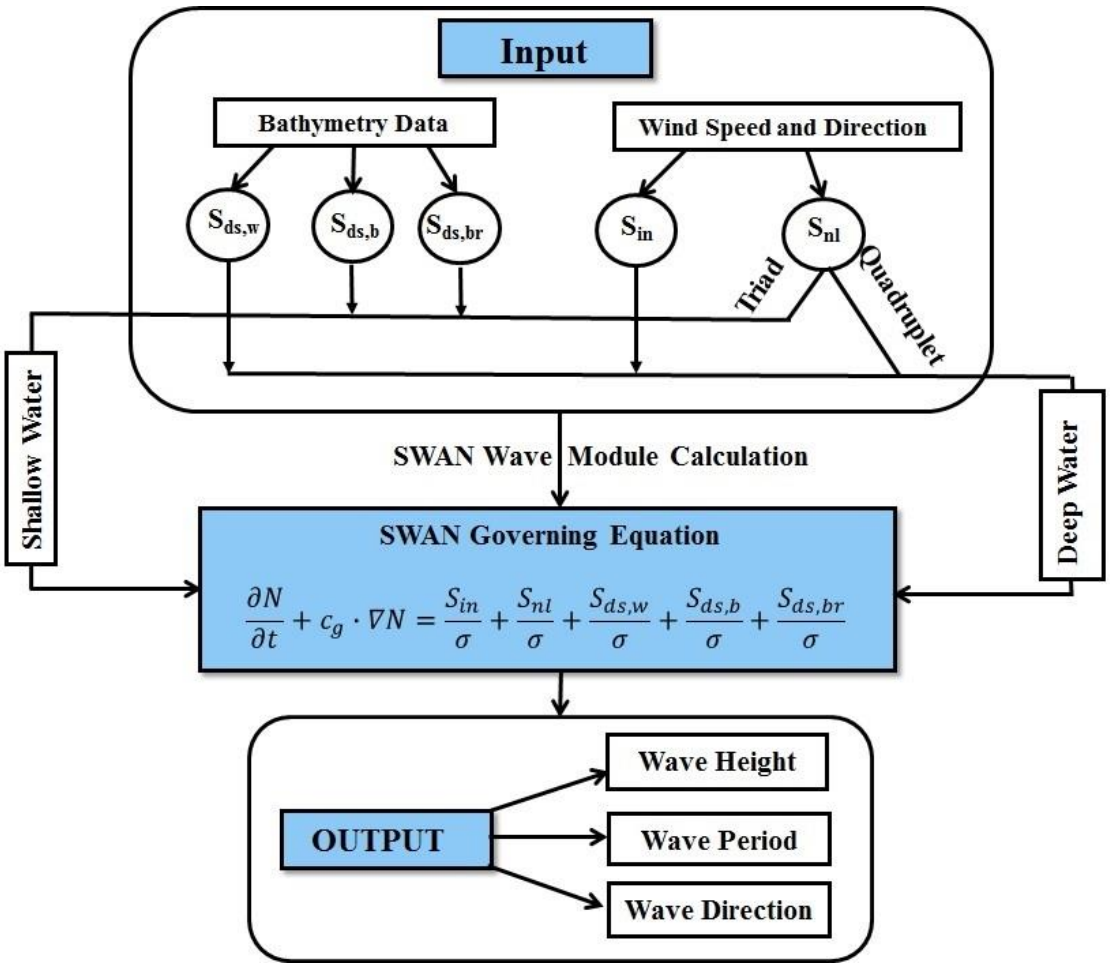

Figure 2.8 The SWAN model configuration with governing energy balance equation

Three processes energy dissipation are considered in SWAN, namely white-capping, bottom friction and depth-induced wave breaking. Bottom friction dominates in shallow water, whereas white-capping is the main source of energy dissipation in deep water. Energy is transformed between waves by non-linear interactions. In shallow water, triad wave-wave interactions play a major role and alternatively in deep water, wave spectrum is dominated by the quadruplet wave-wave interactions.

2.4 Model Setup

2.4.1 Weather Simulation by WRF

In this study, the Advanced Research WRF (ARW) dynamical core was utilized to simulate the atmospheric conditions. The ARW dynamical core considers advection, pressure gradients, Coriolis forces, buoyancy, filters, diffusion and time stepping processes. The atmospheric conditions are reproduced in terms of different parametrizations of meteorological components such as cloud, vapour, water particles, and heat in atmospheric layers. The computational domain covered the entire BOB between 0°N -27°N, 77°E – 103°E, as shown in Figure 2.9.

2.4.1.1 Sensitivity Analysis

To attempt to accurately reproduce cyclone Nargis, a total of 8 WRF sensitivity runs with two different microphysics schemes and four initial run times were conducted, in order to obtain a cyclone track and pressure time history that accurately reproduced historical observations. For each microphysics scheme, the parameterizations and interactions of the hydrometeorological components of the model vary. The two microphysics schemes chosen for simulating cyclone Nargis were Eta (Ferrier) and WSM6 microphysics. The former accounts for water vapor, cloud water, rainwater, and snow while the latter considers two additional parameters: ice and graupel (NCAR, 2017). Detailed information on selected run times, initial and boundary conditions, as well as other modeling schemes are presented in Table 2.2.

Table 2.2 Initial and boundary conditions for WRF simulations of cyclone Nargis

WRF model (Version 3.8)	
Time windows	i) 00:00 UTC 29/04/2008 – 00:00 UTC 04/05/2008
	ii) 12:00 UTC 29/04/2008 – 00:00 UTC 04/05/2008
	iii) 00:00 UTC 30/04/2008 – 00:00 UTC 04/05/2008
	iv) 12:00 UTC 30/04/2008 – 00:00 UTC 04/05/2008
Domain area	Latitude: 0°N -27°N
	Longitude: 77°E - 103°E
Centre of domain	14°E, 90°E
No. of grid points	Horizontal - 230 points
	Vertical - 250 points
Resolution	9 km
Time step	30s
Microphysics	i). Eta (Ferrier) scheme (Rogers et al., 2001)
	ii). WSM6 scheme (Hong and Lim, 2006)
Land surface option	Noah land surface scheme (Tewari et al., 2004)
Radiation	RRTMG long and short wave (Iacono et al., 2008)
Planetary boundary layer	YSU (Hong et al., 2006)
Cumulus parameterization	Kain-Fritsch (Kain, 2004)

The track, minimum central pressure and maximum wind speed of cyclone Nargis that was reproduced by WRF were compared with observed data from the India Meteorological Department (IMD). The weather station data in Myanmar is not freely accessible and recordings are conducted with a 6 hour intervals. Given the lack of reliable records of wind data over Myanmar, the WRF results were compared with the Global Forecast System (GFS) wind analysis data, where 6 offshore locations were chosen. The GFS wind data is also used to force the WaveWatch 3 (WW3) model and is available with a 0.5 degree resolution in the global domain.

As mentioned earlier, the FNL based meteorological dataset was used to produce the WRF wind output, and therefore the two wind datasets were compared to check the potential accuracy of the wind forcing data being introduced into SWAN from WRF subsequently. Both FNL and GFS analysis data are based on the same observational data sources and assimilation system, except FNL, which is run 60-90 minutes behind GFS, using approximately 10% more real data than GFS. Therefore, essentially FNL data quality is slightly superior to GFS (Peng, 2014).

2.4.2 Wave Simulation by SWAN

The WRF model generated two horizontal wind components, u_{10} and v_{10}, along the x (positive values from west to east) and y axis (positive values from south to north), respectively. The wind output was given at 10 m above the surface level with an hourly interval (Skamarock et al., 2008). This wind field output from WRF was used to force the SWAN model. Non-stationary SWAN wave simulations were performed on a spherical coordinate system, with the domain area being slightly smaller than that of the WRF simulation (see Figure 2.9).

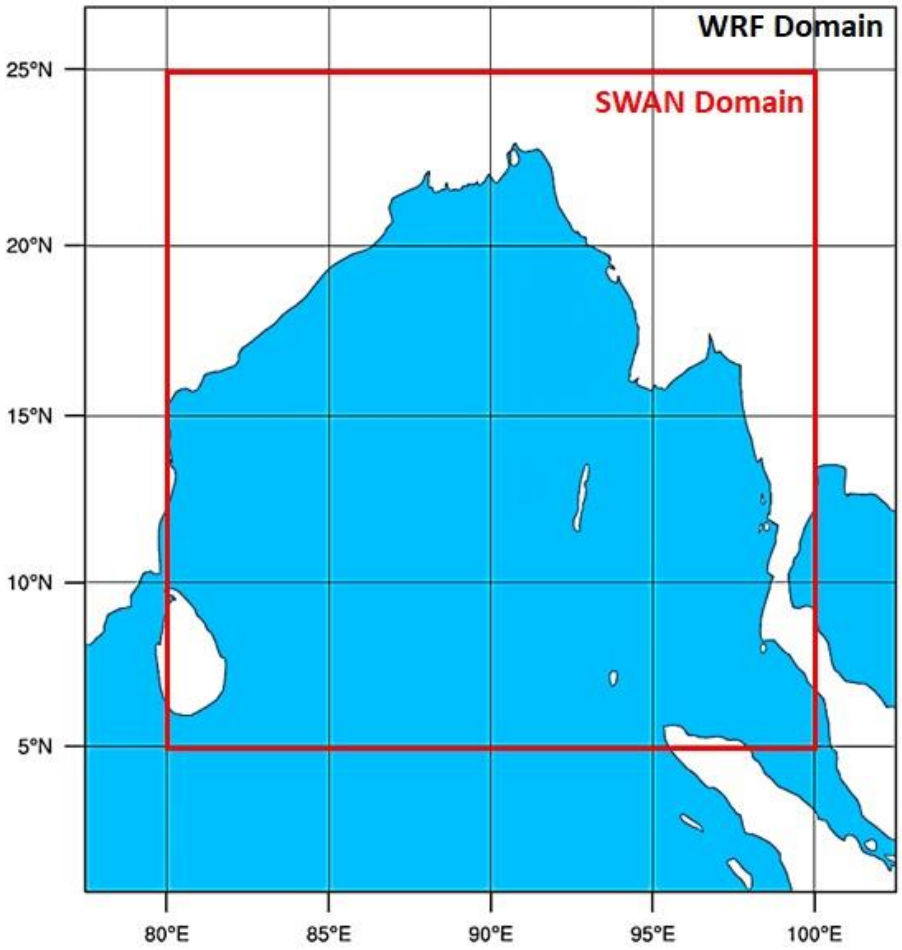

Figure 2.9 The WRF and SWAN domain configurations

The computational grid resolution was set to match the grid resolution of GEBCO's 30 arc-second bathymetry data. For wind and wave directions, the Cartesian convention (anticlockwise from the East) was used. Other numerical options to incorporate physical processes such as non-linear interactions, depth-induced wave breaking, bottom friction and white-capping were also activated, following the recommendations by the SWAN team (SWAN, 2009). Moreover, the model was confined by land boundaries at the East, West and North directions, and by a water boundary at West and South West (see Figure 2.9). The outputs from SWAN include the significant wave heights (H_s), peak wave periods (T_p) and

mean wave directions. The detailed model setup and simulation parameters are shown in Table 2.3.

Table 2.3 SWAN model setup

SWAN model (Version 41.31)	
Domain area	Latitude: 5°N -25°N
	Longitude: 80°E - 100°E
Physical processes	Wave growth by wind (Komen et al., 1984)
	White capping (Komen et al., 1984)
	Bottom friction (Hasselmann et al., 1973)
	Triad interaction (Eldeberky, 1996)
	Quadruplet interaction (Hasselmann, 1985)
	Breaking (Battjes and Jassen, 1978)
Frequency range	0.02 - 1.0 Hz
Frequency division no.	40
Direction division no.	36
Time step	5 min

A time series comparison analysis was performed between the wave output parameters of the SWAN model and the NOAA WW3 model. This is a multi-grid spectral wave model that runs four times a day at nine rectilinear global and regional nested grids, using wind field input from operational GFS analysis at 1 hour interval. For bathymetry, WW3 uses the 1 arc-minute ETOPO-1 dataset from the National Geophysical Data Centre (NGDC) and covers the global domain from longitude 180°E-180°W to latitude 77.5°N-77.5°S. The model provides global simulated wave hindcasts at 3 hour interval with a 0.5 degree resolution from July 1999 to present. Furthermore, along track satellite observed dataset was also utilized for the validation of the SWAN results, given that the accuracy of the satellite measurements of wave parameters has improved in recent times (Bhaskaran et al. 2013; Samiksha et al. 2015; Hithin et al., 2015; Woo and Park 2017). Hence, a correlation analysis of the H_s simulated by SWAN and the along-track satellite measured H_s was also conducted.

2.5 Results

2.5.1 WRF Hindcast Results

Figure 2.10 shows the simulated cyclone tracks, which differ according to the initial simulation times and microphysics (Eta or WSM 6) schemes used, together with the observed track of the cyclone according to the IMD. It can be seen from these figures that the Eta microphysics scheme shows a better accuracy than WSM 6 in terms of track. The main difference between the two microphysics schemes is that Eta does not account for ice and graupel, while WSM 6 does (NCAR, 2017). Since the current simulation area (BOB) is mainly influenced by tropical and subtropical climate, the contributions of ice and graupel parameters from WSM 6 microphysics are not significant for this region, explaining why Eta produces better results.

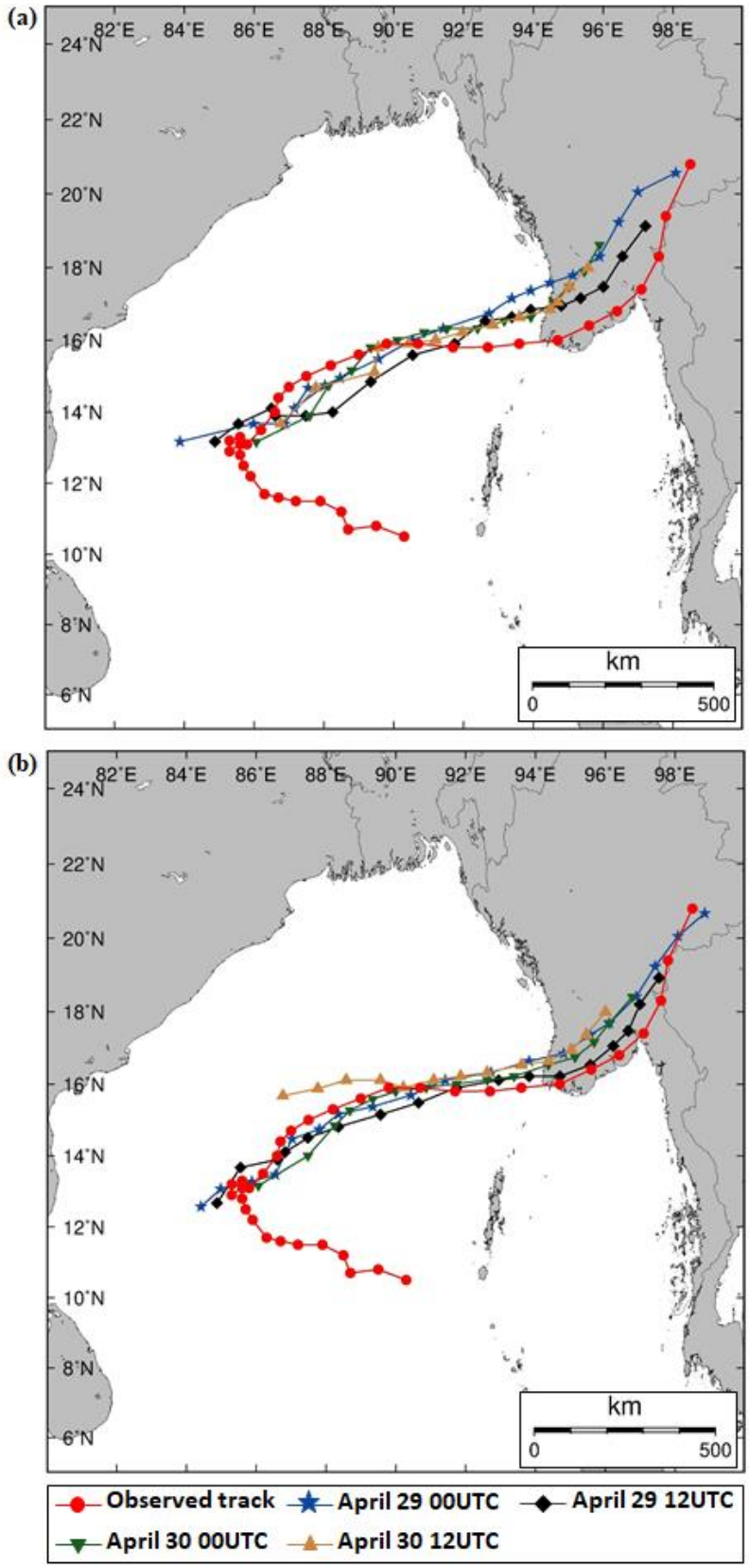

Figure 2.10 WRF simulated cyclone Nargis tracks at four different initial simulation start times (a) using WSM 6 microphysics, (b) using Eta microphysics

The sensitivity analysis also showed that the initial simulation times control the simulated cyclone track, especially the landfall location. With Eta microphysics, the initial calculation time starting from 12 UTC 29 April 2008 (70 hours before the actual landfall time of 10 UTC 2 May 2008) outperforms the other simulations. Also, it resulted in the minimum landfall location (18 km) and cyclone arrival time (1 hr) deviation errors, as compared to the observed historical cyclone (see Figure 2.11). This suggests that, in WRF, it is important to set a proper initial simulation time (48 to 72 hours prior to the actual landfall time) as it can largely affect the hindcast cyclone track accuracy.

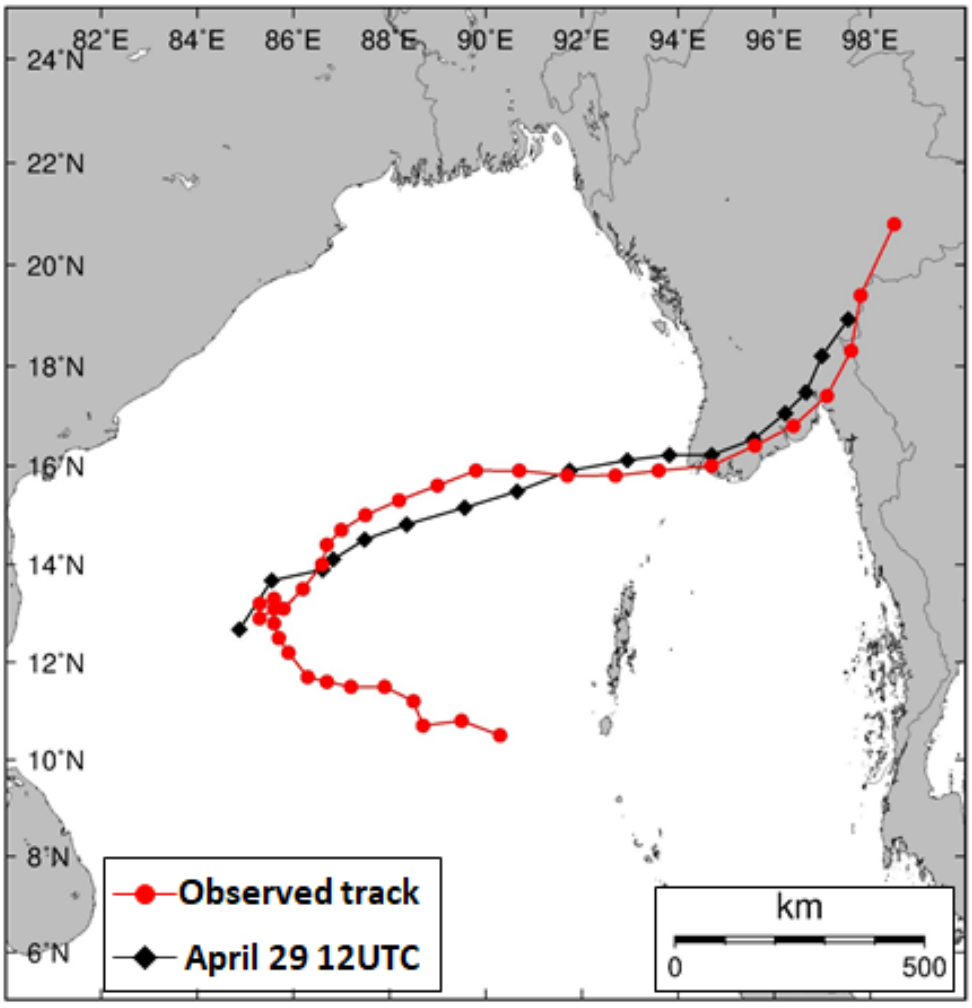

Figure 2.11 WRF simulated track of Nargis with Eta microphysics scheme, from which the resultant wind fields were obtained as input for the SWAN wave simulation

For the WRF simulated cyclone track in Figure 2.11, the comparison of cyclone central pressure at mean sea level and the wind speed with the observed data by the IMD is depicted in Figure 2.12. Although the WRF simulated central pressure and wind speed deviate from the observed data during the early simulation period, the model could at least reproduce the minimum central pressure (at 962 hPa) and maximum wind speed (at 41 m/s), in close agreement with values given by the IMD. For the simulation of wind waves, the wind field over the entire domain is more influential than the meteorological properties at the centre of the cyclone itself. Therefore, the hourly wind field extracted from the WRF simulation, starting at 12 UTC 29 April 2008 with Eta microphysics scheme, was used as a wind forcing input for wave simulation in SWAN.

(a)

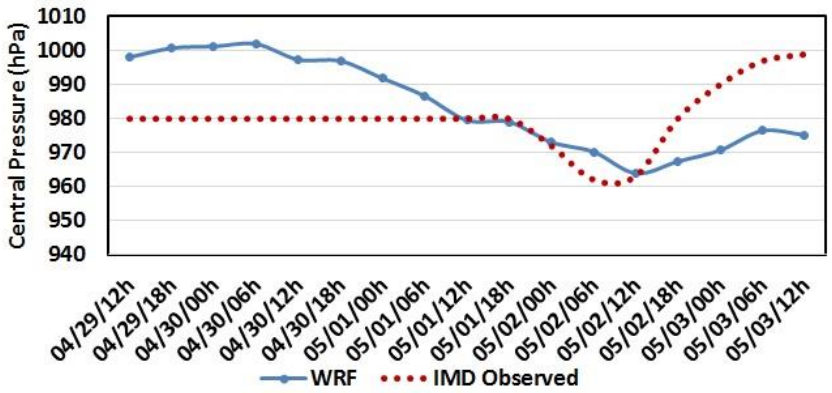

(b)

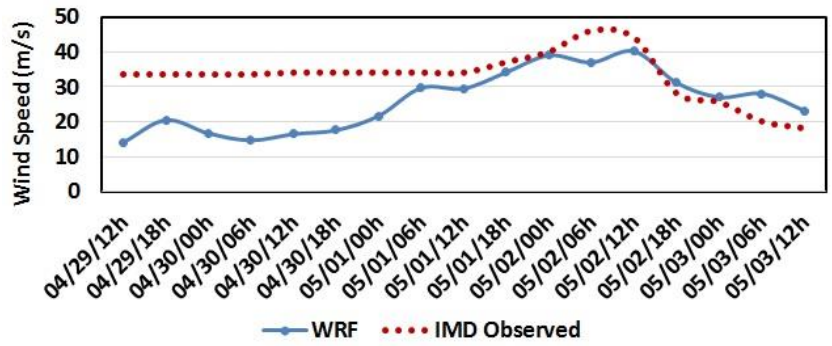

Figure 2.12 Comparison between WRF and IMD observed (a) central pressure and (b) wind speed

Six offshore points in the vicinity of cyclone Nargis track, near the Myanmar coast, were selected for wind and corresponding wave comparisons. These points were chosen to represent the various depths from shallow (16 m) to deep (2001 m) water, that influence the different wave properties around the cyclone affected deltaic coast. Figure 2.13 and Table 2.4 indicate the geographic locations and associated water depth at the selected points. Figure 2.14 shows a comparison of the wind speeds (W_s) and wind directions (W_{dir}) between WRF and GFS, indicating that they agree well for all six offshore points. The small deviations in Ws are likely because of downscaling the 1 minute resolution FNL data to 9 km resolution grids. Furthermore, the physics schemes and other WRF settings can influence the results to various extent. Since the validations are not conducted with in-situ observations, the author acknowledge the lack of reliability regards to actual simulation accuracy.

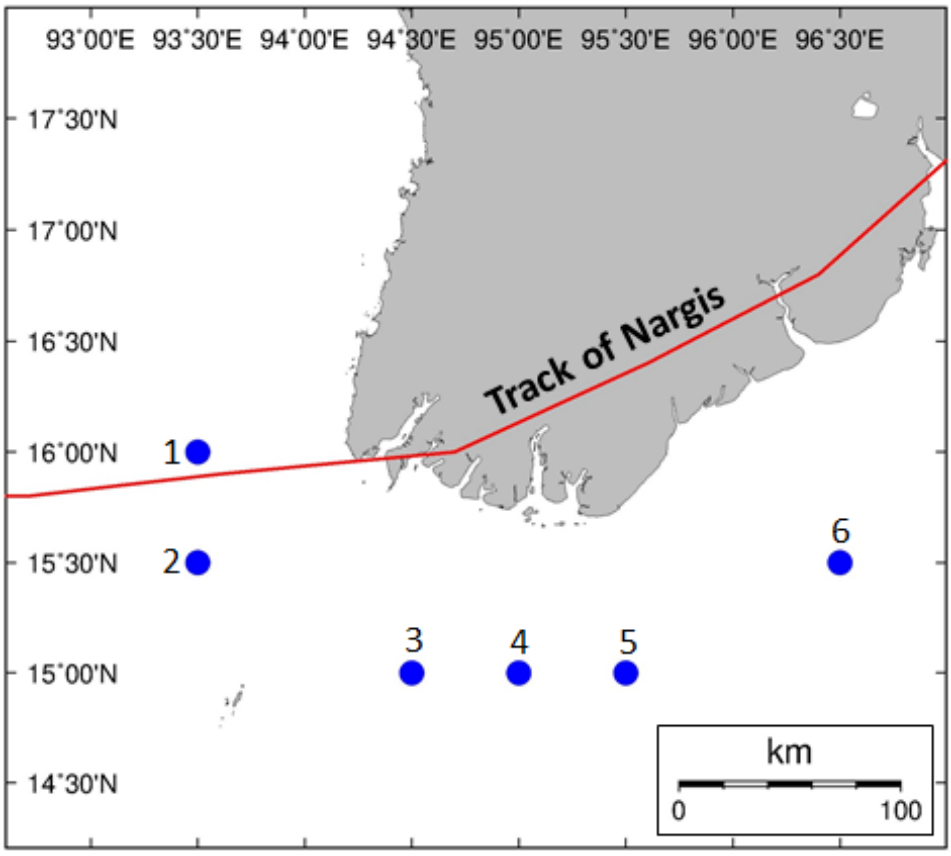

Figure 2.13 Locations of the six offshore points selected for the model comparisons

Table 2.4 Geographical location and depth of offshore points for model comparisons

No.	Geographic Location	Water Depth (m)
1	93.5°E 16°N	2100.7
2	93.5°E 15.5°N	1523.3
3	94.5°E 15°N	56
4	95°E 15°N	49.7
5	95.5°E 15°N	78.6
6	96.5°E 15.5°N	16.6

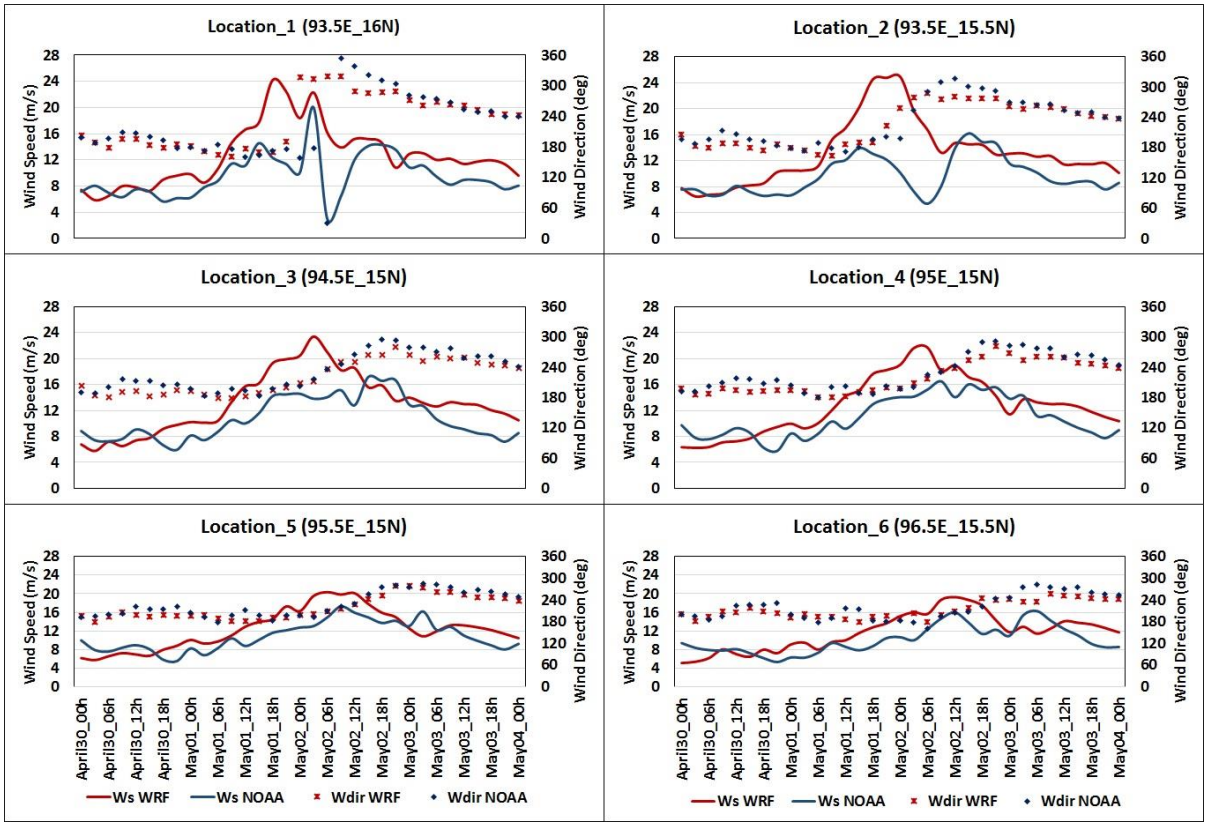

Figure 2.14 Comparison of wind speeds and directions between NOAA and SWAN at selected offshore locations

2.5.2 SWAN Hindcast Results

SWAN wave simulations were carried out by using the hourly wind field output from the WRF simulation (Eta microphysics scheme) with 12 UTC 29 April 2008 as the initial simulation start time. A snapshot of the wave field simulated by SWAN over the calculation domain at 22 UTC 1 May 2008 is given in Figure 2.15, which clearly showed the high wave field generated by Nargis. At 00 UTC 2 May 2008 (10 h before Nargis made landfall), a maximum H_s of around 5.5 m was computed near the cyclone center (offshore of the Ayeywarwady coast). Throughout the simulation period, H_s of between 3.5 m and 5.5 m were mostly computed in the vicinity of the cyclone. The maximum H_s over the entire simulation period across the computation domain was 7.3 m, at around 22 UTC 1 May 2008 (12 h prior to cyclone landfall time).

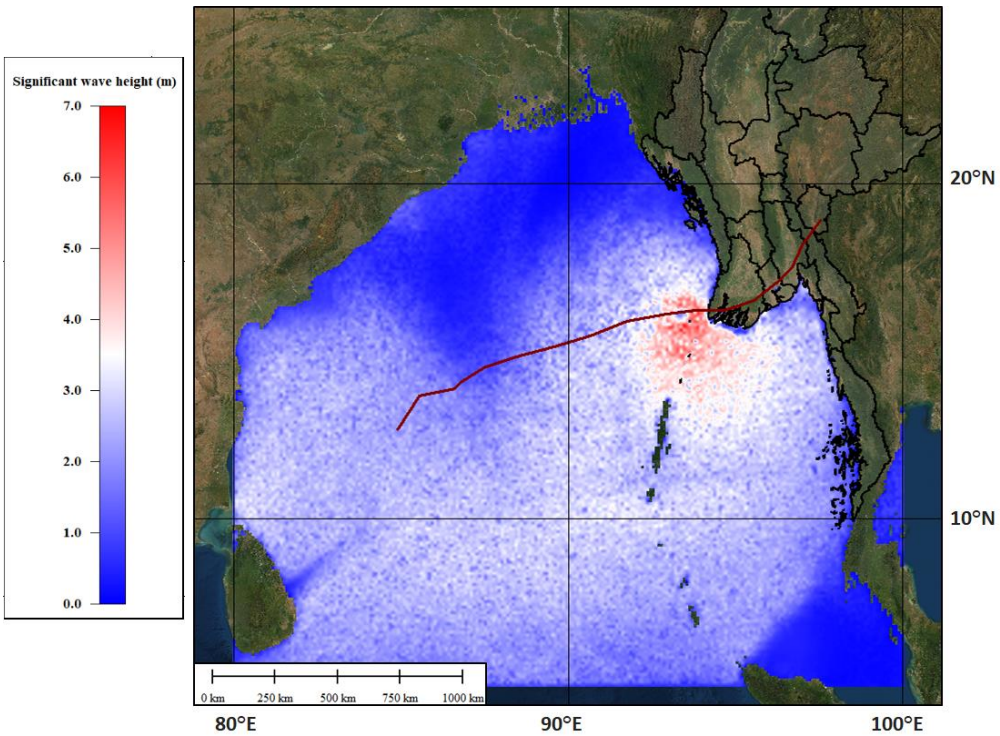

Figure 2.15 Snapshot of significant wave height (H_s) simulated by SWAN at 22 UTC 1 May 2008; red line shows the cyclone track

2.5.2.1 Comparison with NOAA WW3

The time series comparison of significant wave heights (H_s), peak wave periods (T_p) and mean wave directions between the SWAN hindcast and the NOAA WW3 model at the selected offshore locations (see also Table 2.4) is shown in Figure 2.16 (a-f). The main difference between SWAN and NOAA WW3 model relate mainly to the modelling setups, such as bathymetry, spatio-temporal resolutions and simulation time steps. A 30 arc-sec regional domain with 5 minute temporal resolution was used for SWAN, whereas 1 arc-minute global domain with 3 hour temporal resolution was applied in NOAA WW3 (a much coarser resolution). From 00 UTC 30 April 2008 to 00 UTC 4 May 2008, the SWAN calculated H_s values agree well with WW3 wave estimates, in terms of both temporal variations and peak values at all six locations. Maximum H_s values of 5 m were computed at locations 1 and 2 on 18 UTC 1 May 2008, 5 m and 4.2 m at locations 3 and 4 around 06 UTC 2 May 2008 and approximately 4 m at locations 5 and 6 on 12 UTC 2 May 2008.

With regard to the peak wave periods (T_p), the maximum T_p calculated by SWAN was lower than that provided by WW3. The T_p values by SWAN at all locations range from 4 s to 6 s, while those calculated by WW3 have a maximum of 18 s at locations 1 and 2, as shown in Figure 2.16 (a, b). However, at locations 3, 4 and 5, the two models showed similar results, with minimum and maximum differences in T_p of 1 s and 4 s, respectively. The difference in the extent of the computational domains, the sources of wind forcing (GFS and FNL) and other computational physics between the two models are likely to be behind this disagreement in T_p values.

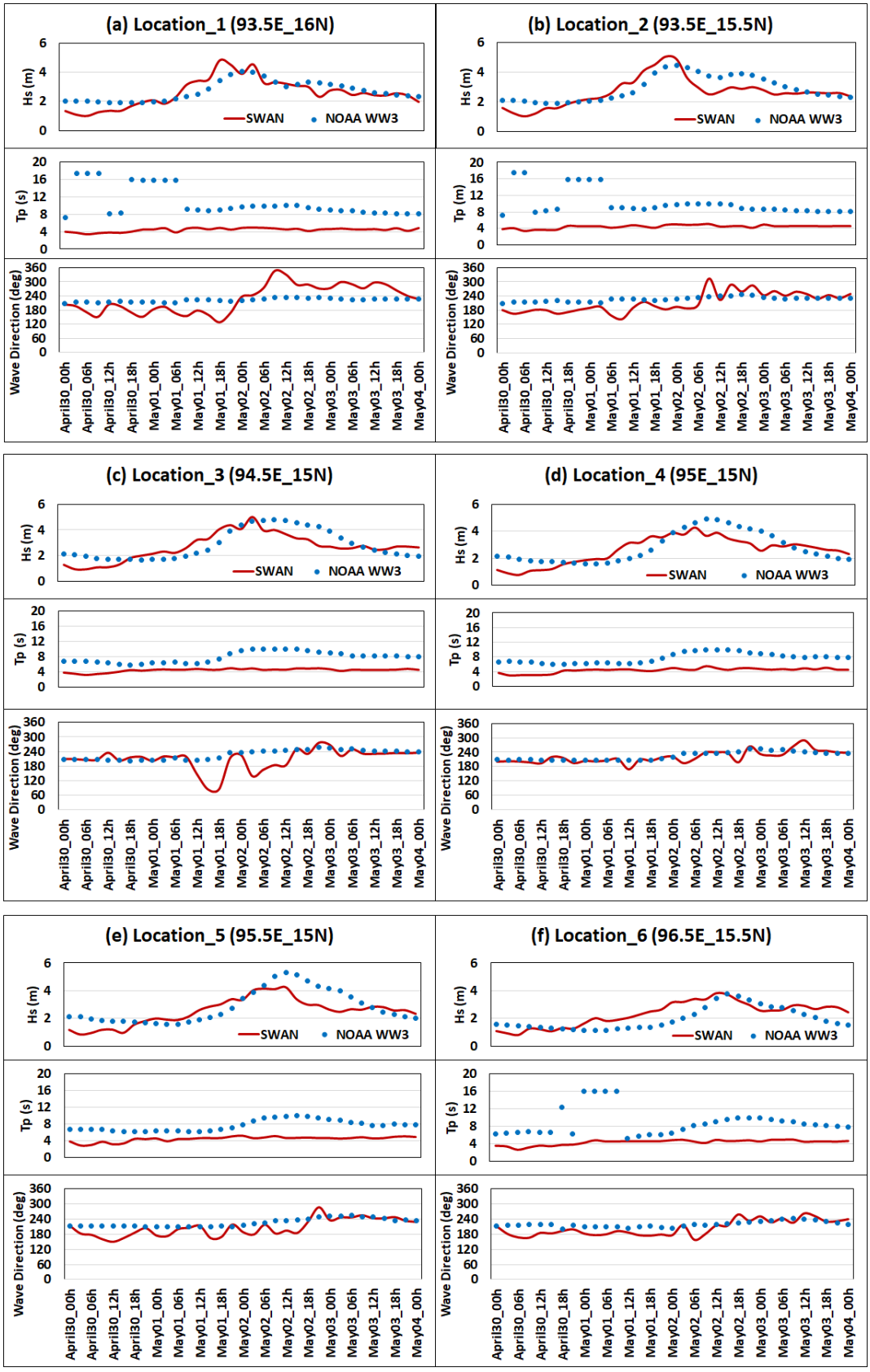

Figure 2.16 Comparison of H_s, T_p and wave directions between SWAN and WW3 at (a) Location 1, (b) Location 2, (c) Location 3, (d) Location 4, (e) Location 5 and (f) Location 6

For the case of mean wave directions, both model results show similar trends. SWAN was able to derive temporal fluctuations in wave direction while the WW3 results show more generalized alternations. This is most likely due to SWAN using a finer GEBCO bathymetry (30 arc-second resolution) than WW3 (1 arc-minute ETOPO-1). At the early stages of cyclone Nargis, the waves were predominantly approaching from the South, and as the storm approached landfall (and after this) the wave directions changed to Southwest, West and Northwest. In conclusion, the performance of the SWAN model appears to be similar to that of the global wave model (WW3 by NOAA), despite the fact that the simulations are executed in a local domain (BOB area), with wind forcing from the locally-run WRF model.

2.5.2.2 Validation with Satellite Wave Data

2.5.2.2.1 Satellite Altimetry Waves

Along-track satellite altimetry wave height data, surveyed by various satellites orbiting the Earth, can be used as an attempt to validate the results of the present SWAN wave simulations. The past, current, and future missions (1959-2043) include over 700 satellites which are operated by different authorities worldwide with the aim of collecting and monitoring data on sea surface, weather and climate (WMO, 2018). The satellites measure the wave height by calculating the time it takes a radar pulse to make a round-trip from the satellite to the sea surface and back (Challenor and Srokosz, 1991). Both the historical and near-real-time calibrated satellite wave products are available from various online repositories (e.g. Globwave, AVISO, NOAA etc., Ribal and Young, 2019). The calibration of the recorded wave products from different oceanographic satellites are also conducted with the in situ buoy data from the National Data Buoy Center (NDBC). The Root Mean Square

(RMS) errors of the corrected linear regression for Jason-1/2 wave height data are found to be 0.27 m and 0.23 m, respectively (Chen et al. 2017).

2.5.2.2.2 SWAN Vs. Satellite Observed Wave Height

In the present study, the final analysis (Level 2 Pre-processed, L2P) wave height datasets derived and extracted from historical Geophysical Data Record (GDR) of the GlobWave database (Farquhar et al., 2013) were used for H_s correlation analysis. General information on the four satellites that crossed near Myanmar coast, in the range of 90°E - 99°E and 10°N - 22°N, during the SWAN simulation period of 30 April to 3 May 2008, is given in Table 2.5. The official agencies that manage these four satellites include the National Aeronautics and Space Administration (NASA), Centre National d'Études Spatiales (French National Centre for Space Studies; CNES), European Space Agency (ESA), US Navy and National Oceanic and Atmospheric Administration (NOAA).

The detailed crossing times of each satellite with each given track number are shown in Table 2.6, and the significant wave heights (H_s) recorded along each track are depicted in Figure 2.17. From Table 2.6, it can be seen that the respective satellites crossed over the vicinity of Myanmar coast only for a very limited time a day. Since a 5 minute simulation time step was defined for SWAN, the results were thus comparable with satellite altimetry wave data. NOAA WW3 has a coarser temporal resolution (3 h), which means only wave data at 0 h, 3 h, 6 h, 12 h, 15 h, 18 h and 21 h are accessible and none of them agree with the satellite crossing times. It should also be noted that since the tracks of ENVISAT and ERS-2 cross over each other (Roca et al., 2009) with a certain time difference, their tracks share the same geographical area but have different labelled track numbers (30B vs. 30C, 1A vs.1B, and 2A vs. 2B), as shown in Table 2.6 and Figure 2.17.

Table 2.5 General information of four satellites that crossed near Myanmar coast between 30 April to 3 May 2008

Satellite	Period of operation	Name	Agency	Repeat cycle
JASON-1	07/12/2001 - 01/07/2013	Joint Altimetry Satellite Oceanography Network-1	NASA/ CNES	9.9156 days
ENVISAT	01/03/2002 - 08/06/2012	ENVironmental SATellite	ESA	30-35 days
ERS-2	21/04/1995 - 06/07/2011	European Remote Sensing-2	ESA	35 days
GFO	10/02/1998 - 26/11/2008	Geosat Follow-On (GEOSAT: GEOdetic SATellite)	US Navy/NOAA	17 days

One limitation of the satellite data is the coarse apposition of measurement points (Hithin et al., 2015) due to the along track orbital movement of satellites over the globe (refer to Figure 2.17). Given this, a total of 295 measurement points were available for comparison with the SWAN results following the temporal and spatial adjustments of data distribution between the two datasets within the simulation domain. Specifically, these 295 comparison points consist of 35 points from ERS-2, 133 points from ENVISAT, 68 points from JASON-1 and 59 points from GFO.

Table 2.6 Approximate times of the day that the satellites crossed over the vicinity of Myanmar coast

Date	Track no.	Time (UTC)	Satellite
	30A	04:30:00	JASON-1
30/4/2008	30B	15:40:00	ENVISAT
	30C	16:10:00	ERS-2
	1A	04:05:00	ENVISAT
1/5/2008	1B	04:35:00	ERS-2
	1C	17:10:00	JASON-1
	2A	03:35:00	ENVISAT
2/5/2008	2B	04:05:00	ERS-2
	2C	11:25:00	GFO
3/5/2008	3A	15:40:00	ENVISAT

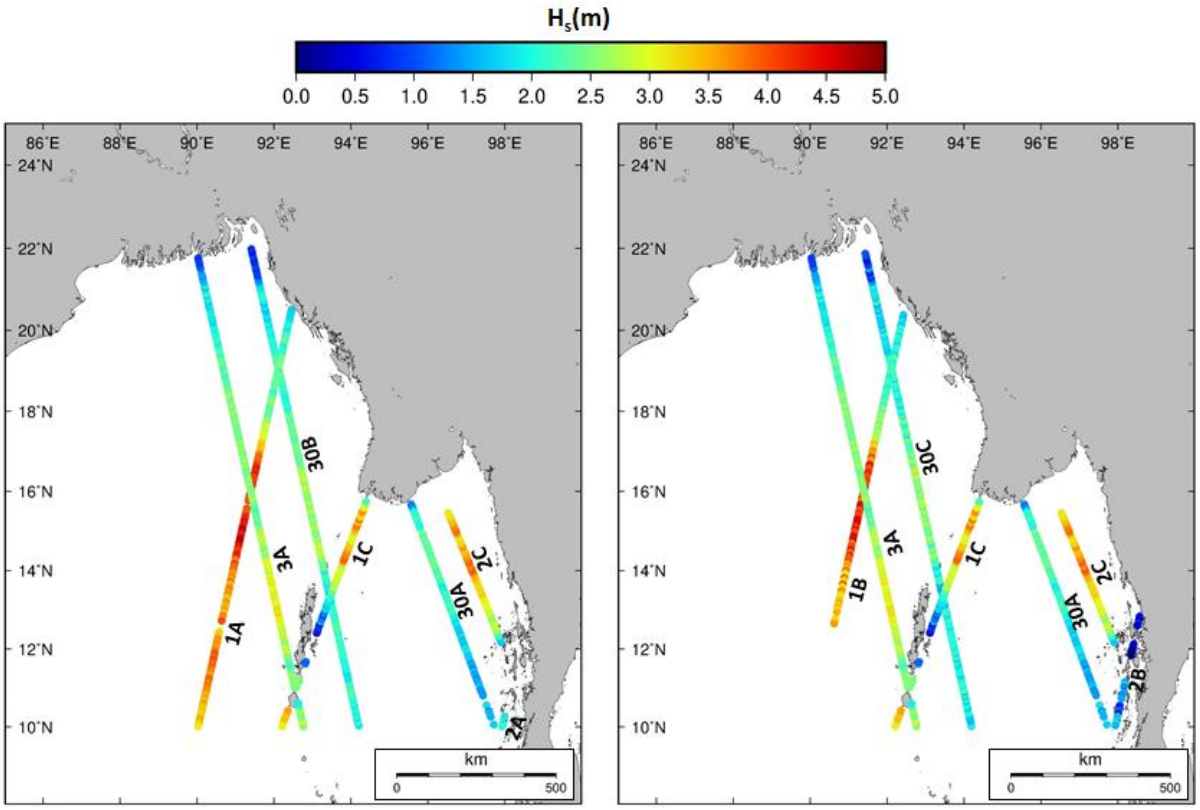

Figure 2.17 Along-track satellite recorded H_s in the vicinity of Myanmar coast from 30 April to 3 May 2008

Figure 2.18 shows the H_s correlation between the calculated SWAN simulations and the satellite measurements, showing a relatively good fit with a correlation coefficient of 0.89. The maximum H_s was found to be around 4 m in both the SWAN and satellite H_s. For reference, other recent studies of long and short term validation of satellite wave data with in-situ wave buoys at different regions worldwide show accuracies ranging from 80 to over 90% (Hithin et al., 2015; Woo and Park, 2017). Hence the present study is at the upper range of what can be expected in terms of accuracy, especially for higher H_s values which is the dominant factor for the design of coastal structures and planning of the coastline compared to the normal seasonal low waves.

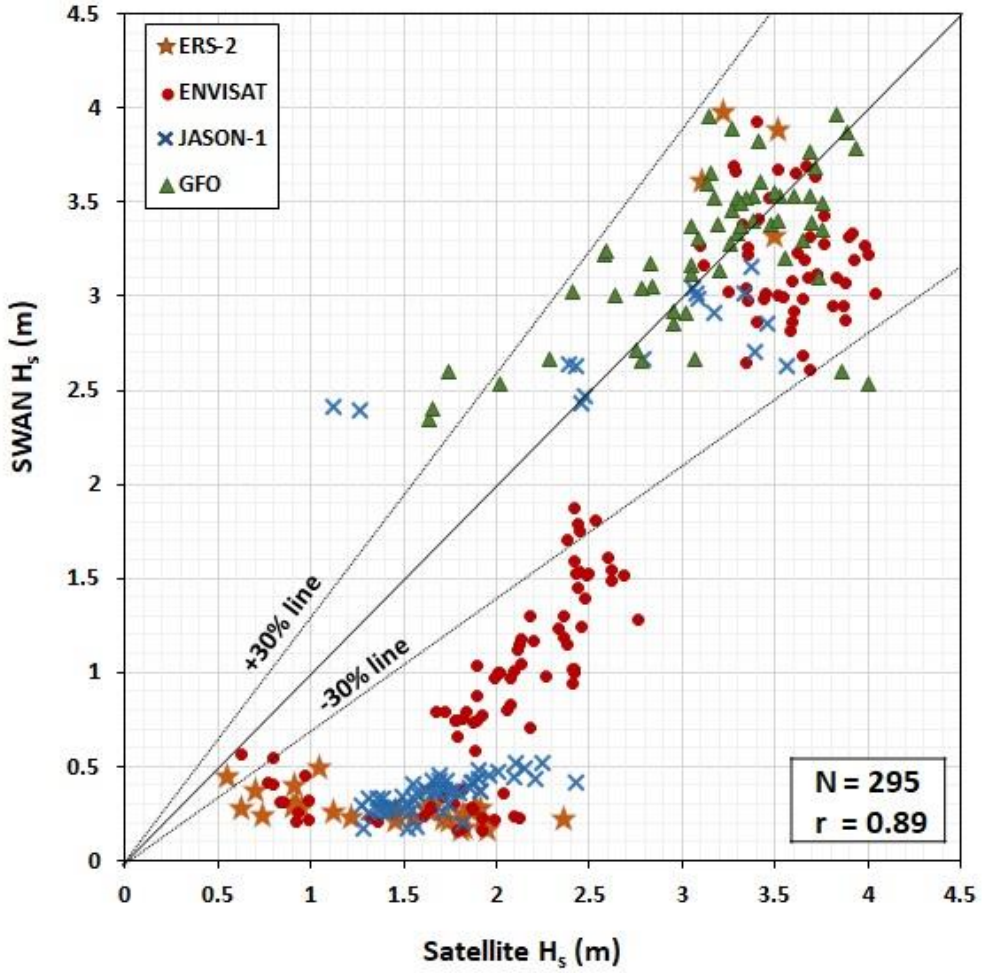

Figure 2.18 Correlation analysis between SWAN simulated H_s and satellite measured H_s

Among all the satellite data in the present work, the correlation obtained was better between high H_s values than the lower ones. As mentioned above, the wind forcing for the wave simulations in SWAN was extracted from the initial WRF run, which is known to have limitations for weak synoptic flows during the warm-up period of cyclones (Islam et al., 2015; Nakamura et al., 2016). This results in an underestimation of H_s by SWAN, compared to the satellite results. Hence, the integrated WRF-SWAN model has some limitations when trying to estimate low wave conditions. In addition, there are problems for the estimation of H_s by SWAN and the satellites in shallow water areas, due to rapid changes in bathymetry.

Nevertheless, the high correlation between the SWAN H_s and satellite altimetry can partially validate the accuracy of the wave simulations conducted and the reliability of the model.

2.6 Discussion

In May of 2008, an extreme cyclonic storm, Nargis, made landfall in Myanmar and caused coastal flooding and damage along the deltaic coast of the country. A top-down numerical approach using a combination of weather (WRF) and wave (SWAN) modelling techniques was applied to simulate cyclone Nargis and its wind-generated waves. The WRF model can reproduce the cyclone well, with its track and intensity agreeing well with observed data by the IMD. A sensitivity analysis of the WRF results indicates that it is better to use the Eta microphysics scheme over the BOB, where tropical and subtropical monsoon climate characteristics are dominant. The starting simulation time of WRF highly influences the simulated cyclone track, and in this case the simulation starting about 70 hours prior to the actual time of landfall results in a cyclone track with a minimum landfall displacement error of 18 km.

According to the SWAN simulation, waves with a maximum H_s of 7.3 m were generated offshore of the deltaic coast of Myanmar (Ayeywarwady and Yangon) during the passage of the cyclone. This value is four to five times higher than the seasonal monsoon waves generated at this coastline, where low to moderate energy waves are the norm. The major port of Myanmar (Yangon Port), which accounts for more than 90% of maritime imports and exports (MPA, 2020), is situated in the Yangon area. Therefore, it is recommended to establish a wave observation station near Yangon river mouth to obtain data from such extreme events in the future.

Most of the time, cyclonic waves arrive from the southwest direction, being similar to those of normal monsoon waves. However, there was a quick change in wave direction from 180 to 240 degrees (south to southwest) before and after the landfall of cyclone Nargis. The maximum T_p was simulated to be 5.6 s. The SWAN simulated H_s have a correlation coefficient of 0.89 when compared with the satellite recorded H_s, with there being a closer agreement between the higher values than the lower ones. Hence, this highlights the potential for this integrated model to be used in the prediction of the more extreme waves that are possible around the coastline of the country.

Since Myanmar lacks a dense network of wave observation stations, the numerical modelling methodology used in this research represents a powerful technique to identify peak wave heights during cyclones. Likewise, satellite wave products can be used to assist in such efforts to hindcast the significant wave height along the coastline of the country, as well as to provide near-real-time warning of extreme wave conditions. This is important not only for the initial planning of coastal infrastructure (given that there are few or no long time series data of in-situ observations), but also to ensure the safety of coastal communities in this low-lying area. Since it is highly possible that a strong TC like Nargis could take place again in the future (as the event has a predicted return period of around 1 in 100 years, Tasnim et al., 2015b), there could be higher waves induced by stronger wind fields which lead to even more destruction. Therefore, effective countermeasures should be put in place to reduce the disaster potential to coastal communities in Myanmar.

3 Development of a Deep-learning Based Wave Forecasting Model and Its Application at Japan Coast

3.1 Introduction

Real-time wave forecasting is of utmost importance for the planning and operations of offshore construction and maintenance projects, as the accurate prediction of when low waves will take place is essential to decide whether work will proceed. The origins of wave forecasting date to empirical formulations in the early 1940s (Sverdrup et al. 1947) and was then followed by the development of first, second and third generation numerical wave models (Mandal and Prabaharan, 2010). The accuracy and usefulness of such numerical wave models have been widely reported all over the world. However, they are known to be computationally expensive and time-consuming, as they require solving physics-based numerical equations and extensive bathymetry and meteorology datasets (O'Donncha et al. 2018), which becomes a clear downside especially when a real-time wave prediction is necessary.

Nowadays, Artificial Neural Networks (ANNs) have become popular in wave forecasting, due to the technological advancement and availability of long-term wave data records (Deo and Naidu, 1998). Over the years, a number of machine learning wave forecasting models have been developed, and their integrated usage with physics-based numerical models has become popular (James et al. 2017, O'Donncha et al. 2018). Kim et al. (2016) predicted storm surges using Feed Forward Neural Networks (FFNNs) at Tottori coast, Japan, and Tracey et al. (2019) applied Convolutional Neural Networks (which can be also categorized as one type of FFNNs) to predict wave characteristics of the Japan Sea using meteorology data. Other ocean wave studies using ANNs include predicted approximation of non-linear source term of energy balance equation of wave spectra by Tolman et al. (2005),

or time series of significant wave height forecasting by using wavelet and ANN hybrid model by Prahlada and Paresh (2015). In general, most recent studies apply FFNNs, with an emphasis on the prediction of the time-series of waves. However, FFNNs are known to be related with vanishing and exploding gradient problems for the prediction of time-series data, since the information flows only in one direction from inputs to outputs (Brezak et al. 2012).

In the present thesis, the author thus follow a different approach, a deep-learning-based wave forecasting model was developed for the classification of waves using Recurrent Neural Networks (RNNs). In RNNs, unlike FFNNs, the internal memory can be used and thus the output of the network is influenced by not only the current input but also the previous inputs/outputs (Brezak et al. 2012). Specifically, the Long Short Term Memory (LSTM) network, which is a type of RNNs, was used in the current research. The LSTM network (Hochreiter and Schmidhuber, 1997) consists of internal contextual state cells of long-term or short-term memory, meaning that the model can perform predictions, utilizing the information used not only in the very last step (short-term) but also previous steps (long-term) through integrating loops.

As a case study, the model was utilized to predict the wave conditions at two locations along the Japan coast. The training and testing of the model was conducted to predict both low and high wave conditions, with the practical aim of being able to inform practicing engineers on how to predict in advance whether it would be possible to conduct offshore construction work or not. Thus, while advancing knowledge about deep-learning-based wave predictions in the field of coastal engineering, the research presented also has concrete applications that can help engineers currently working in the Japanese coastal and offshore construction industry. The accurate prediction of low wave conditions is important for the day-to-day planning of offshore and nearshore construction work, and the present model represents a practical tool to reduce the potential waste of resources in such projects.

3.2 Study Area and NOWPHAS Wave Data

Japan is a complex archipelago formed by a multitude of islands, bays and inner seas. Generally speaking, the wave climate in the inner seas is mild, and the study of the areas facing the open sea is more important from a project construction and operation perspective. The part of the Japanese coastline that is facing the open sea can be divided into two geographically distinct regions (see Figure 3.1):

i) The Sea of Japan in the west side, which in the present work will be represented by the town of Tottori.

ii) The Pacific Ocean side, where Kashima was chosen as a case study location.

The input wave data was obtained from the Nationwide Ocean Wave information network for Ports and HArbourS (NOWPHAS) under the Port and Airport Research Institute, Japan (Nagai 2000). The data consists of significant wave height (H_s), significant wave period (T_s) and wave direction being recorded at 2 h time interval at each observation point (NOWPHAS maintains a large number of buoys and other recording instruments throughout the Japanese coastline). The wave data was recorded with doppler-type directional wave meter at both locations.

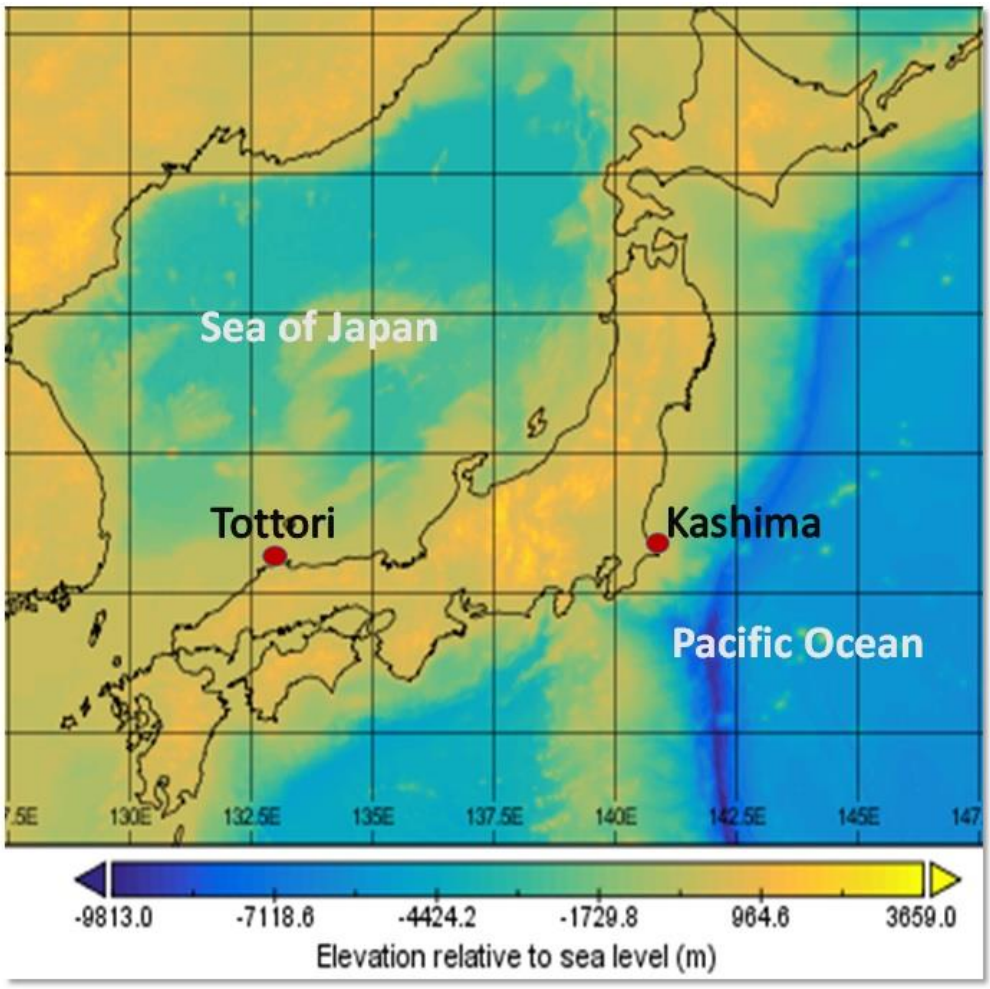

Figure 3.1 Map of part of the Japanese archipelago and surrounding seas, indicating the location of the case study locations

Five-years equivalent of wave data at each location was used as input into this research, with the total number of data points count and the percentage of the year that this represents (in terms of the availability of the data) being shown in Table 3.1. Essentially, these measuring stations can sometimes break, particularly during the passage of strong typhoons, tsunamis or for a number of other causes. For Tottori, nearly 100% of the wave data is available annually from 2011 to 2015 (in other words, wave data is available for every two hour of the year for most years). For the case of Kashima, facing the more inclement Pacific Ocean (from where typhoons approach), since only 17.83% data is available for the

year 2011, the wave data for 2010 (with 81.74% availability) was also included to obtain the five-years equivalent wave data.

Table 3.1 Annual wave data availability at each location

Year	Tottori		Kashima	
	Number of data points	**Availability (%)**	**Number of data points**	**Availability (%)**
2010			3580	81.74%
2011	4379	99.98%	781	17.83%
2012	4375	99.61%	4392	100%
2013	4376	99.91%	4375	99.89%
2014	4380	100%	4380	100%
2015	4380	100%	4376	99.91%

The distribution of H_s and T_s is shown in Figure 3.2, which provides an overall view of the wave characteristics offshore of Tottori and Kashima. Generally, lower-energy waves are more common at the Japan Sea side than the Pacific Ocean side, where seasonal high waves due to typhoons and swells are dominant (Shimura and Mori, 2019). Accordingly, in Figure 3.2, the maximum recorded H_s in Kashima is approximately 2 m higher than that in Tottori, and similarly the difference in T_s is around 5 s. Moreover, Tottori is characterized by frequently having waves with H_s below 0.5 m and T_s between 4 to 6 s, while in Kashima H_s around 1 m and T_s around 8 s are most common. The waves direction also agrees with the locations of Tottori and Kashima (Figure 3.1). Accordingly, waves coming from north, north-east and north-west are dominant in Tottori and those approaching from west, west-northwest and west-southwest in Kashima.

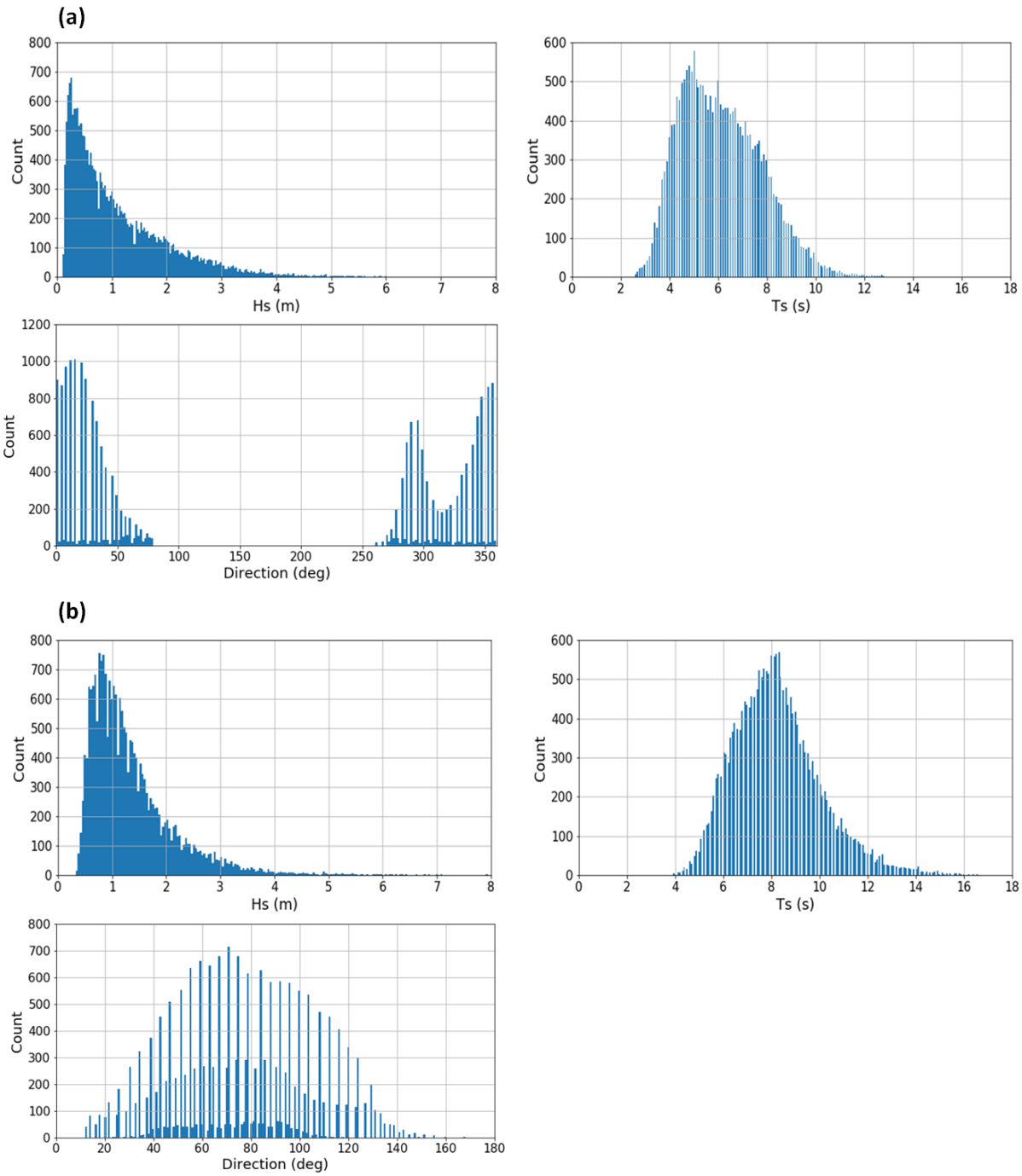

Figure 3.2 Distribution of H_s, T_s and wave direction at (a) Tottori (2011-2015) and (b) Kashima (2010-2015)

3.3 Method: Deep-learning Model Framework

Figure 3.3 shows the general flow of a machine learning (deep-learning) model framework. The data cleaning is the most important pre-processing process before feeding the inputs to the network, since the accuarcy of the model highly depends on the input data quality and distribution. After pre-processing, the corresponding design network simulations are carried out thorugh thousands of iterations where the hyper-parameter tuning takes place to achieve a better accuracy of the prediction model. At the final stage, the validation of the deep learning model is conducted by adjusting the loss between simulated and observed data.

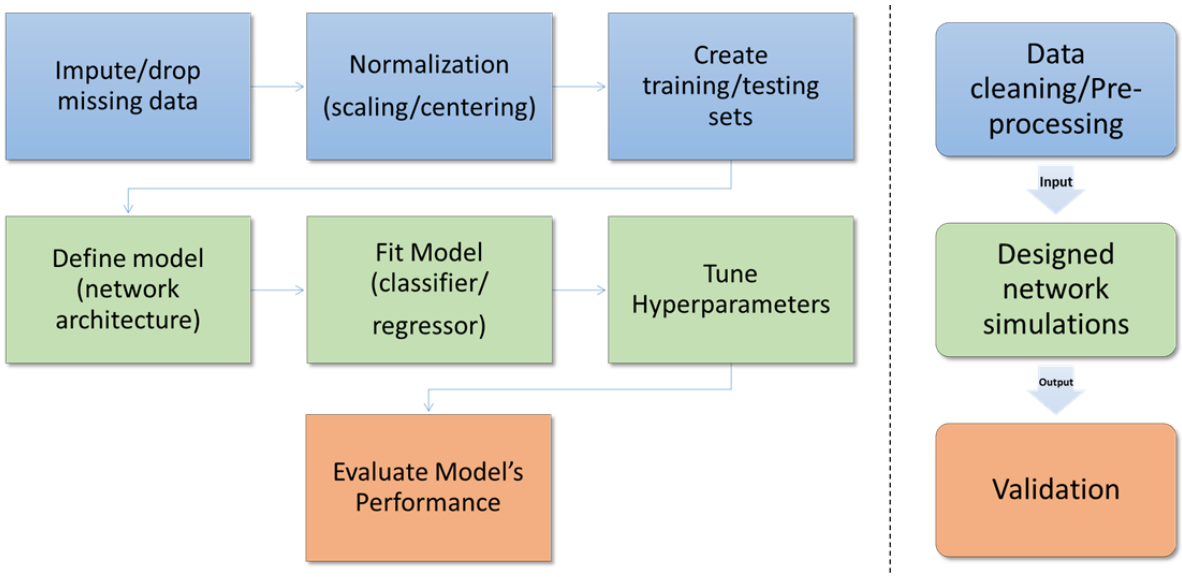

Figure 3.3 General flow of a deep-learning model development

In this study, since the time-series wave data is available as known inputs and outputs (a set of labelled data), a supervised learning method where the training model learns the labelled training data with desired output to predict the future unseen values was used (Raschka and Mirjalili, 2017). Based on the direct mathematical relationship between inputs and outputs, the model can be used for categorical classification with discrete class labels. As

shown in Figure 3.4, the relationship between various input features is extracted from labelled training data, which then provides an output. This model output is then adjusted with the existing output in the original dataset by means of error (loss) evaluation and the corresponding weight and bias of the training model are updated to optimize the accuracy of the model. Finally, when the minimum error and maximum accuracy of the model is obtained, it can be used for actual prediction with new unseen data.

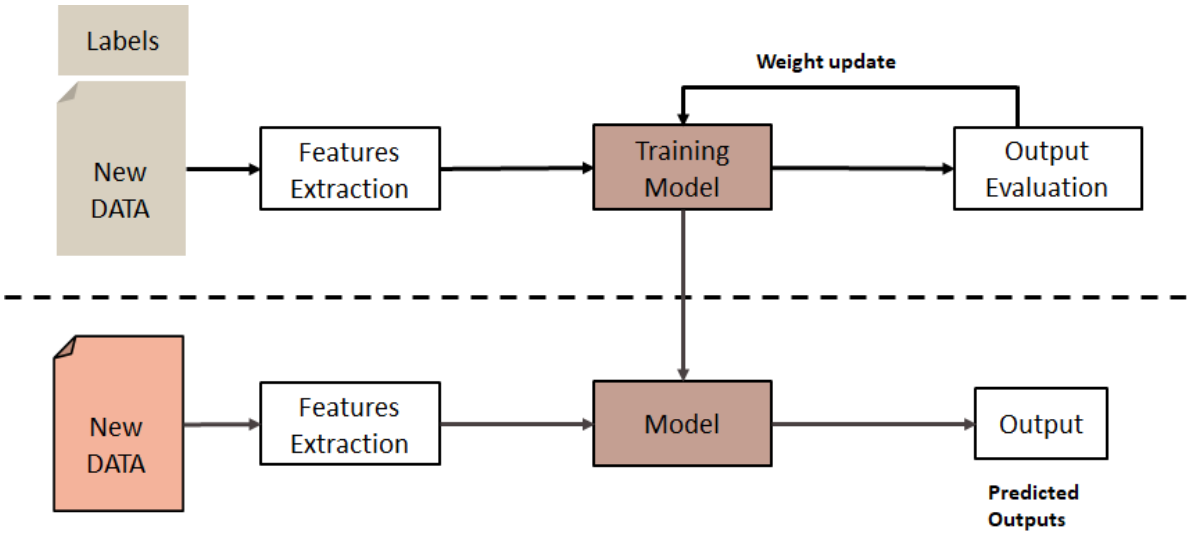

Figure 3.4 Training model development with supervised learning

3.3.1 The LSTM Deep-learning Model

The Long Short-Term Memory (LSTM) used in the present thesis is a commonly used type of RNN, which is suitable for the analysis of problems based on time-series data, as it can utilize inputs/outputs information in previous steps for the prediction in next step (Goodfellow et al. 2016). The general framework of the designed network model is shown in Figure 3.5. The network layers include an input layer, network layers and an output layer. The input layer is the point where the initial features (which correspond to sequential wave heights and periods at a given time in the present simulations) from the dataset are passed to

the subsequent network layers. In order to consider 24 h, 48 h and 72 h sequential inputs, a pre-processing that involved cleaning the outliers from the original wave data and allocation of input arrays with different sizes (respectively for 24 h, 48 h and 72 h) with their designated output labels was performed first.

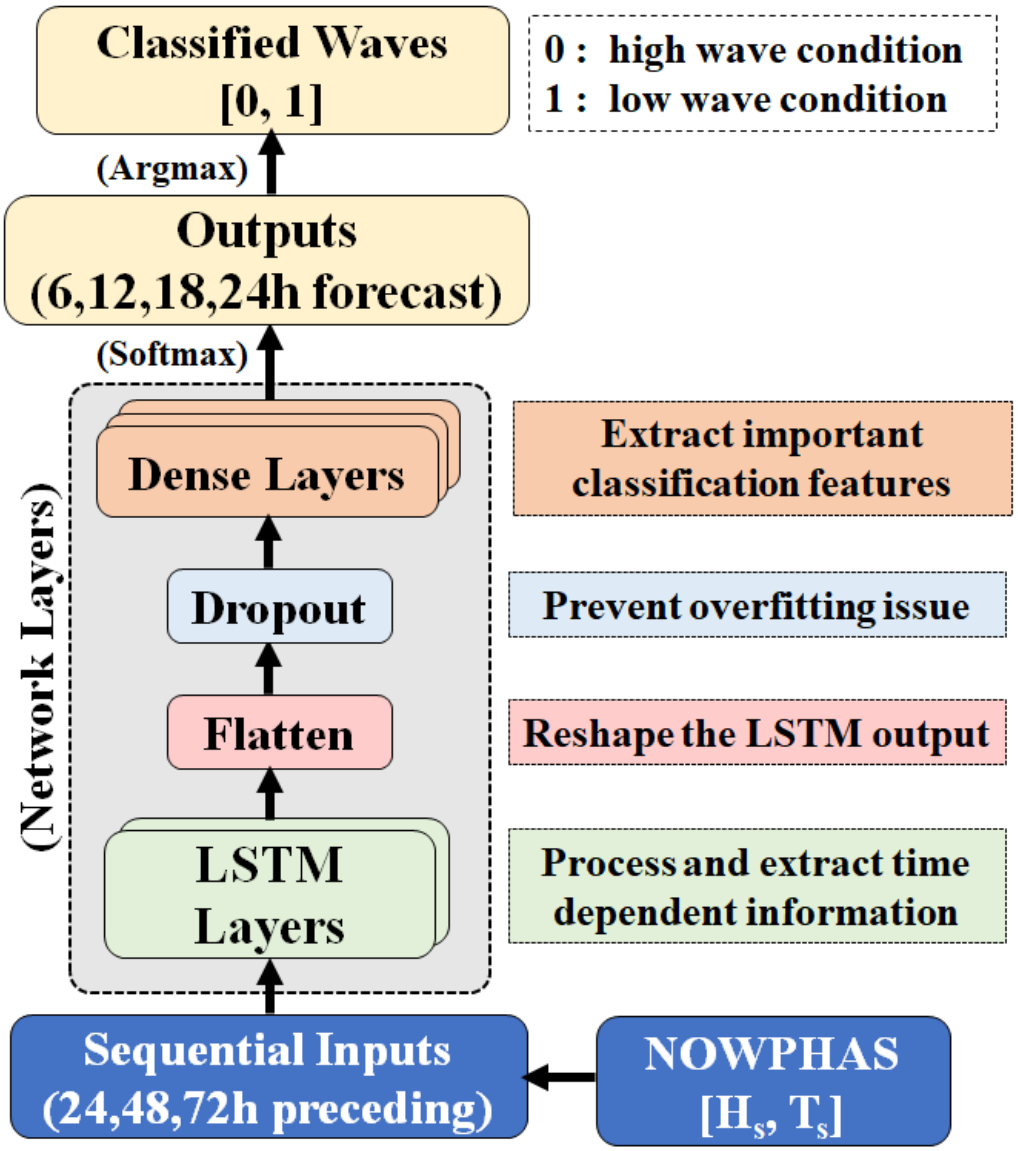

Figure 3.5 Framework of the model

Inside the network, LSTM layers first process the sequential data and extract the time dependent information from the input. The Flatten layer is then added to reshape the hidden (LSTM) layers output, and the Dropout layer is used to prevent overfitting (as a regularization to improve model's generalization ability to new unseen data) (Srivastava et al. 2014 and Zaremba et al. 2014). Subsequently, the Dense layers extract the features information for final classification and the Softmax activation function (Raschka and Mirajalili 2019) is assigned to normalize the probability results in the Dense layers' output arrays. Four different forecast times, of 6 h, 12 h, 18 h and 24 h, are defined in the output layer. Finally, through the Argmax function, which returns the index of the maximum value in an array (0 or 1 in this case), the output layer provides the final classified wave forecast of low and high conditions.

3.3.2 Input Features and Wave Classification Categories

Data regarding the wave parameters H_s and T_s are inputted into the model sequentially. Since a supervised learning method was used in this study, it is necessary to define the class labels beforehand for both the training and testing processes of the model to provide the classification output. Two class labels were thus defined, as shown in Table 3.2, that can help determine whether it will be advisable or not to conduct work offshore or nearshore in the future (as explained later the next day.

- class-0, for high energy waves that do not allow working offshore (including also swells), with either the values of H_s or T_s being greater than 0.8 m and 9 s, respectively.
- class-1 low energy waves, with both the values of H_s and T_s being smaller than 0.8 m and 9 s, respectively

Table 3.2 Classification category for low and high waves based on H_s and T_s

Wave Height (H_s) / **Wave Period (T_s)**	$0 <= H_s < 0.8$ m	$H_s >= 0.8$ m
$0 <= T_s < 9$ s	Low	High
$T_s >= 9$ s	High	High

3.3.3 Simulation with Different Preceding/Forecast Times

To examine the performance of the model, a total of 120 different scenarios were simulated by varying ranges of input and output times and amount of data volumes. As shown in Table 3.3, three designated input times (t), including the preceding 24 h, 48 h and 72 h and four forecasted output times ($t+ \Delta t$) with 6 h, 12 h, 18 h and 24 h ahead were considered. One year to five years' datasets, ranging from around 4000 to over 20,000 samples, were used for each pair of input and output times (12 pairs in total) at each location (see Tables 3.4 and 3.5). Therefore, for the two locations a total of 120 simulations were performed in order to check the sensitivity of the model to different preceding and lead times and data volumes.

The neural network simulation functions and parameters, utilized in all the simulations, are shown in Table 3.6. These include the Softmax function for activation, Categorical crossentropy for loss (error) calculation, and Adam optimizer for tuning of the network to achieve better accuracy at each iteration step. A total of 500 epochs (iterations) with training batch sizes of 100 was considered to cope with catching the minimum loss and maximum accuracy by the network. However, in order to save the time taken by each simulation, the EarlyStopping regularization (Girosi et al. 1995) was added with a patience value of 25, which means that the simulations through the configured network will be

automatically stopped when the validation accuracy is no longer improved after 25 iteration steps. The training and testing data were divided with a common 80/20 ratio, in which 80% of the input was used for training and the remaining 20% for validation of the network.

Table 3.3 Consideration of input/output times and data volumes for model simulations

Time (h)		**Train/test data volume**
Preceding input (*t*)	**Forecast output ($t+\Delta t$)**	**(No. of consecutive years)**
24 h	6 h	1 year
48 h	12 h	2 years
72 h	18 h	3 years
	24 h	4 years
		5 years

Table 3.4 Training and testing datasets for each simulation at Tottori

No. of years	**Samples**	**Train**	**Test**
1 year (2015)	4380	3504	876
2 years (2014-2015)	8760	7008	1752
3 years (2013-2015)	13135	10508	2627
4 years (2012-2015)	17510	14008	3502
5 years (2011-2015)	21890	17512	4378

Table 3.5 Training and testing dataset for each simulation at Kashima

No. of years	Samples	Train	Test
1 year (2015)	4375	3500	875
2 years (2014-2015)	8755	7004	1751
3 years (2013-2015)	13130	10504	2626
4 years (2012-2015)	17520	14016	3504
5 years (2010-2015)	21880	17504	4376

Table 3.6 Network simulation functions and parameters

Activation	Softmax
Loss	Categorical crossentropy
Optimizer	Adam
Callback	EarlyStopping (Patience: 25)
Dropout probability	0.5
No. of epochs	500
No. of batch	100
Train/Test Ratio	80/20

3.4 Results

3.4.1 Simulation process

Depending on the input and output array dimensions and the number of nodes defined at each network layer, the tuning of weights and bias takes place in the hidden layers of the network during the training process. On this process, the model itself attempts to minimize the loss (difference between the predicted and observed output) and maximize the accuracy thorough defined iteration steps in each network layer. Through this trial and error calculation (hyperparameter tuning), the optimized model with best accuracy is obtained.

In the present work, all the network parameters in each layer were fixed, except the dimensions of the input array, which complies with different sequential times of 24 h, 48 h and 72 h. The number of trainable and non-trainable variables (weights and bias) related to each preceding time input is described in Table 3.7. It can be seen that the longer the array dimension of the input layer (preceding time), the larger the number of training variables for optimization of the network and the more complicated the simulation becomes. In Table 3.7, since there are no non-trainable parameters, it can generally be accepted that the deep-learning model's training process was properly conducted to provide reliable forecasting output. The detailed configurations of hidden layers corresponding to each preceding time are depicted in Figure A1, A2 and A3.

Table 3.7 Number of trainable and non-trainable variables (weights and bias)

Preceding time	Trainable variables	Non-trainable variables
24 h	412,612	0
48 h	608,770	0
72 h	805,378	0

3.4.2 Classification Accuracy

All of the simulated scenarios were quantitatively analysed and compared to check the applicability and reliability of the model for wave forecasting. For each scenario, the final classification accuracy of the model was validated by means of a confusion matrix (Raschka and Mirajalili, 2019), which shows a comparison of the predicted classes against the observed ones, as depicted in Figure 3.6. In other words, the confusion matrix indicates how much the model got confused between the defined classes (0 and 1) and the respective observed labels and predicted values.

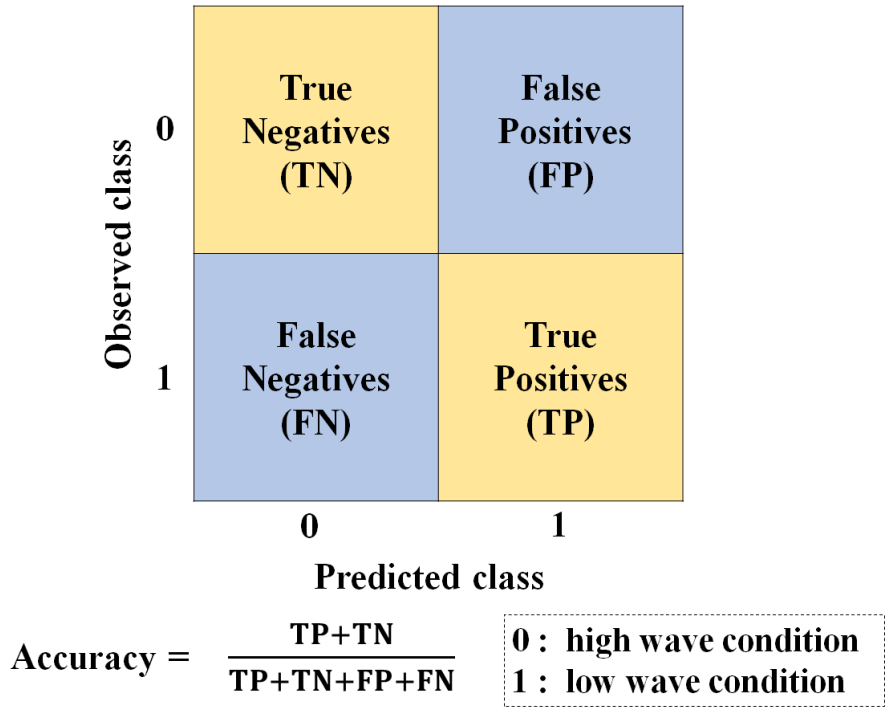

Figure 3.6 Confusion matrix and prediction accuracy of the model

The classification accuracy of the model is defined by the following equation:

$$\text{Accuracy} = (TP+TN) / (TP+TN+FP+FN) \quad (3.1)$$

where TP represents true positives, TN represents true negatives, FP represents false positives and FN represents false negatives. The classification accuracy was obtained by dividing the sum of true positives (class-1) and true negatives (class-0) by the total number of predictions made, in other words, the total entries in the validation dataset.

3.4.3 Wave Classification Results at Tottori and Kashima

Figures 3.7 and 3.8 illustrate the classification accuracy (%) predicted by the model for different input/output times and data volumes at Tottori and Kashima. There are total 12 pairs of three input times and four output times for five data volumes (one year to five consecutive years wave data). The results show an overall accuracy ranging from 65 % to over 95 %. Besides, there is no considerable difference of wave classification accuracy between Tottori and Kashima when using three years or more wave data, despite their dissimilar topographic properties (Japan Sea and Pacific Ocean) and dominant wave characteristics. This indicates that the model can ingest the seasonal wave climate at contrasting geographic location in a consolidated way.

It is generally expected that when the forecast time increases the accuracy would become slightly lower. In fact, this trend appears when one year or two years data were used as input data in (see Fig.5a, for example). However, the present results show that the decrease in accuracy is not significant when over three consecutive years data were inputted. The results also demonstrate that preceding time (24h, 48h, 72h) does not significantly influence the classification accuracy in both locations. Therefore, it appears that if only wave data for the previous day is given, wave forecasts up to 24 h ahead can be well predicted using the model, with more than 80% accuracy if over 10,000 data is used to construct the network.

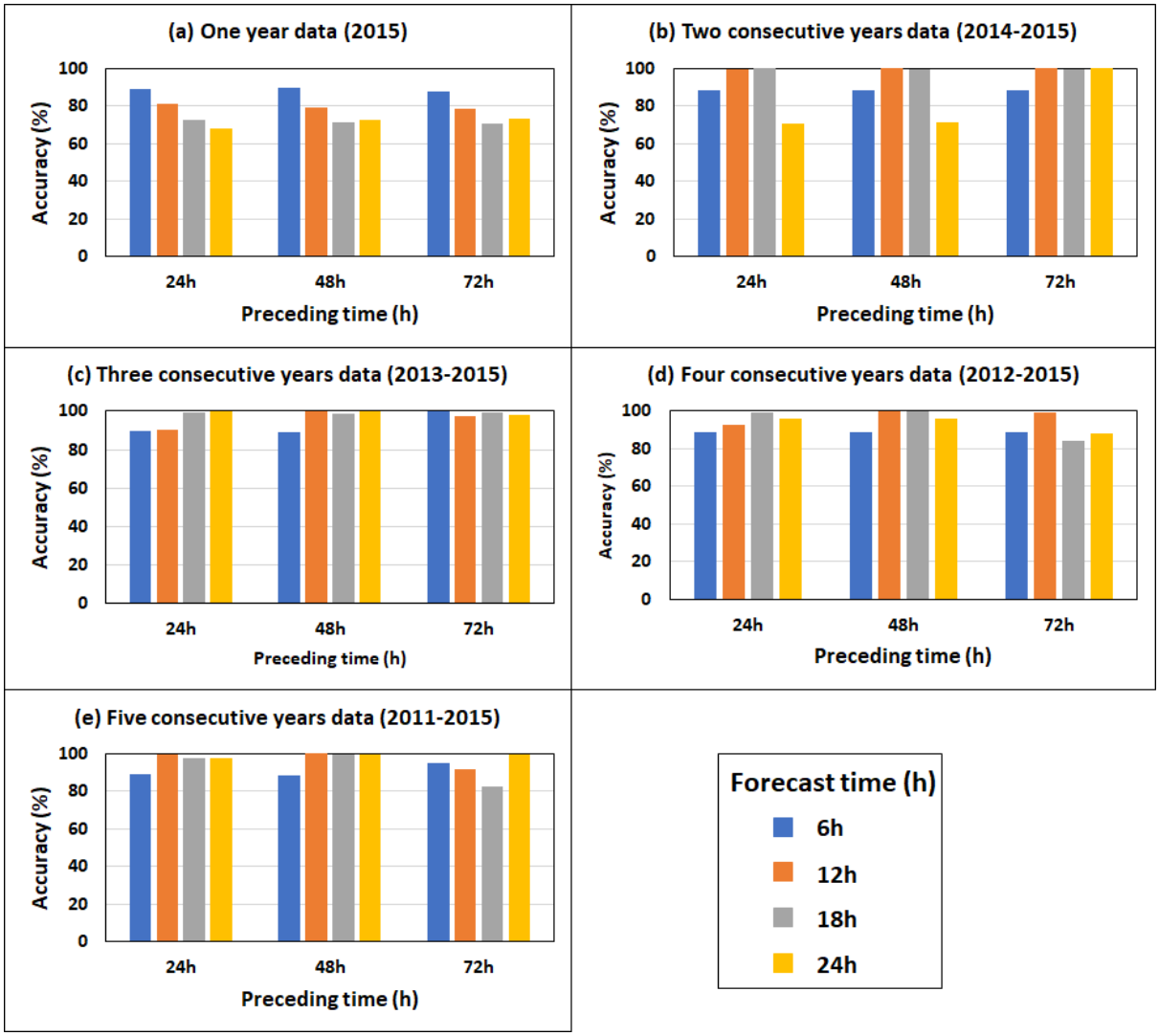

Figure 3.7 Classification accuracy for different preceding and forecast times using five different data volumes at Tottori

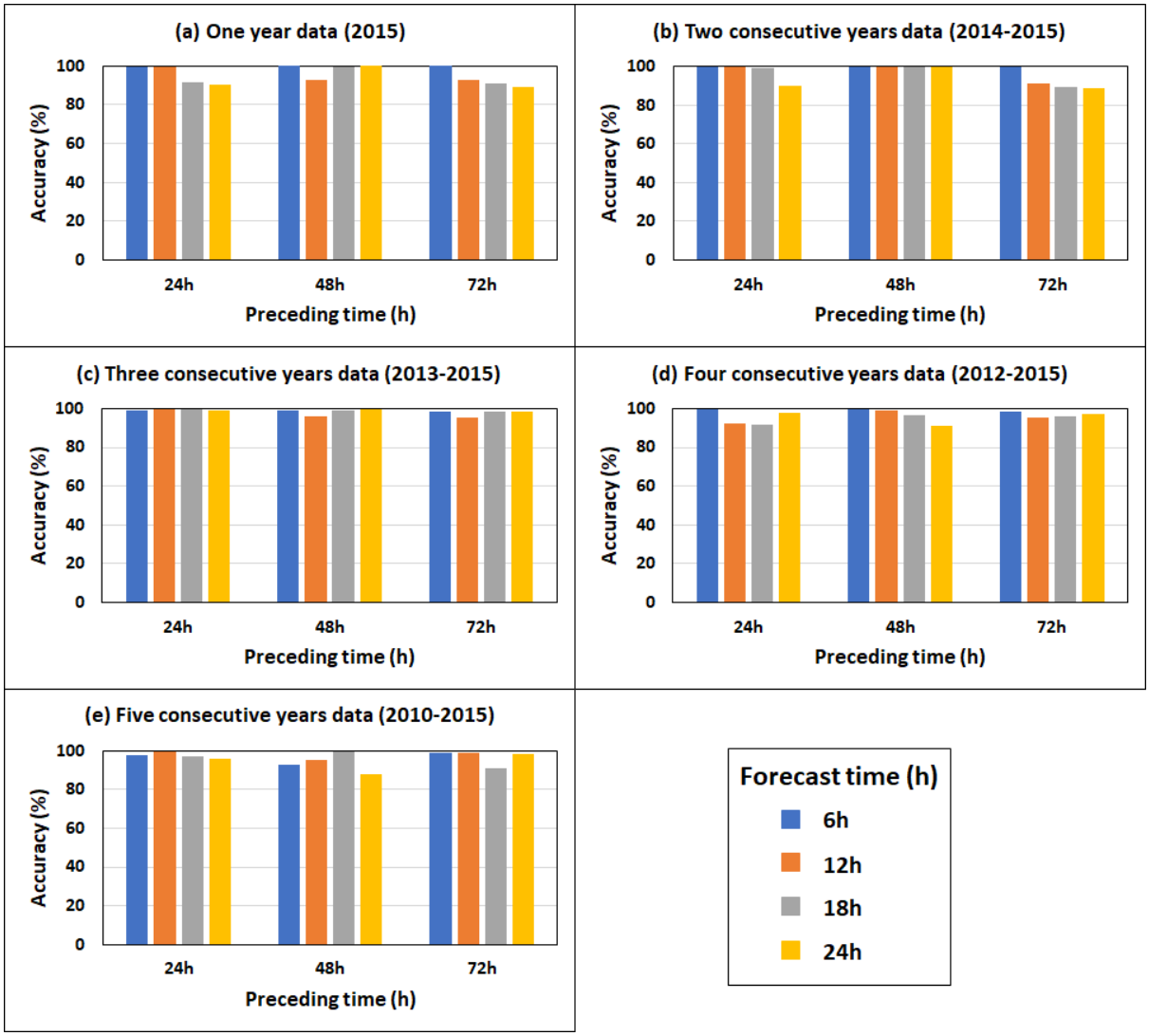

Figure 3.8 Classification accuracy for different preceding and forecast times using five different data volumes at Kashima

In order to compare the all the 120 simulations at each of the two locations, a boxplot of the accuracy according to different data volumes (one to five years) is shown in Figure 3.9. In Tottori, using one-year data results in the lowest accuracy, but for other cases the results show similar average accuracy values (all above 90%), though nearly 70% accuracy was also observed for two years of data. In contrast, in Kashima, the simulations using one-year wave data show a similar level of accuracy to those using larger data volumes, suggesting that the

amount of data necessary for accurate prediction would depend on the locations. At both locations, the simulations (training and testing) of the model with three-year equivalent data results in the highest average accuracy. Overall, the minimum and maximum average accuracy of approximately 78% and 99% validate the reliability of the applied deep-learning model.

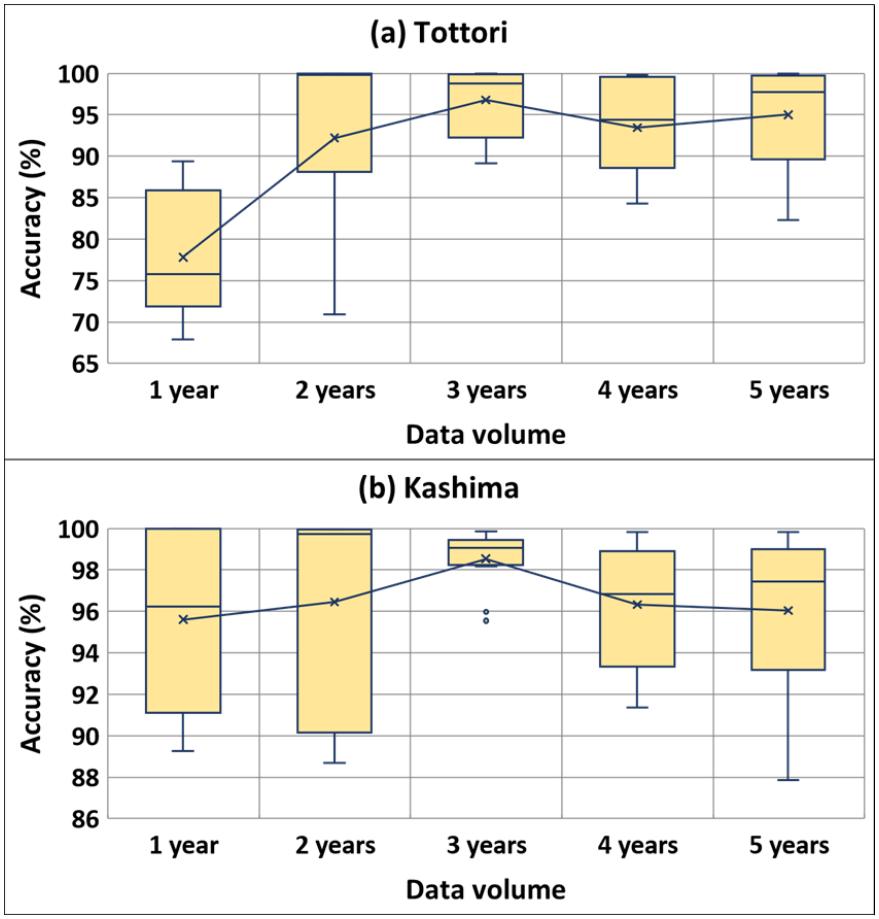

Figure 3.9 Boxplot of accuracy for different data volumes (a) Tottori and (b) Kashima

Figure 3.10 shows the model's performance against the percentage of time when low waves occur (class balance between 0 and 1) in the original wave data. In Tottori, low waves (class-1) take place during 50% of the year, whereas this only happens 20% of the time in

Kashima (which indicates a prevalence of high waves (class-0) in the area). Nevertheless, the average accuracy does not necessarily depend on the class equilibrium, as shown in Figure 3.10. There is no theoretical dependence of the resulted accuracy to the class imbalance especially for the classification problem of machine learning (Juba and Le, 2019). Hence, this specifies the competence of the deep-learning approach used in the present study to the traditional probabilistic approach which is normally applied for conditional forecasting until now. Furthermore, such conditional forecasting has limitations to be conducted by traditional numerical wave models such as SWAN (Booji et al. 1996) and WAVEWATCH III (Tolman, 2002).

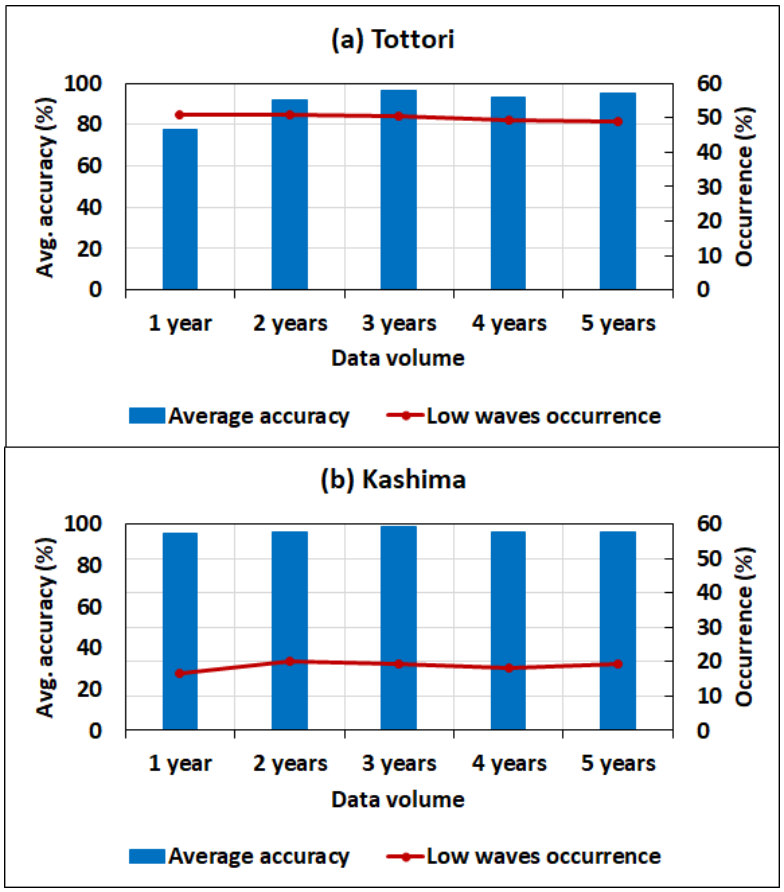

Figure 3.10 Average accuracy vs. occurrence percentage of low waves at (a) Tottori and (b) Kashima

3.5 Discussion

The accurate prediction of wave conditions is essential for the operational planning of offshore construction and maintenance projects. In the present research, a deep-learning-based wave forecasting model using LSTM network, which is a kind of Recurrent Neural Network, was developed to help practicing engineers forecast waves in real-time. In contrast to recent studies of the prediction of time-series of wave parameters by numerical modelling and machine learning, the present study attempted to forecast whether the next day wave conditions would exceed a given threshold value to assist in deciding whether it is feasible to work offshore or not.

3.5.1 Accuracy of the model

In general, high accuracy results were obtained in almost all simulation cases (ranging 75 % - 99 %). Especially, higher average accuracy (around 98%) was obtained for all preceding/forecast times when three consecutive years of wave data was used. The overall results suggest that if the sequential wave data for at least 24 h is known, the wave conditions (low or high) for 24 h lead time can be well predicted by the present model using the minimum three years wave data.

In addition, the classification accuracy does not rely on the percentage of occurrence of low waves in the original wave data at each location. This highlights how the model is potentially applicable to any location in either deep or shallow water, if wave records for at least one year are available. Consequently, given the direct statistical relations of inputs and outputs featured by deep-learning, the model outperforms the ordinary probabilistic approach and numerical wave models in terms of shorter simulation time, fewer number of required

data types and improved applicability. Therefore, the present model can be used as an advanced tool to assist the planning of possible working days at offshore construction sites.

3.5.2 Limitations

In the present study, deep-learning model simulations were conducted at two locations only (Tottori at Japan Sea side and Kashima at Pacific Ocean side). However, it would be preferable to include additional locations to assure the model's reliability as a further study. The model results show the lowest accuracy 67% at Tottori when one- and two-years' wave data were used. It is recommended to use a minimum of 3 years wave data when applying the current model to assure its reliability.

In addition, although the single threshold value of of H_s and T_s was considered in the current research, it is also possible to consider alternate threshold values for different applications, such as the prediction of long period waves or swell. Furthermore, since the simulation parameters are fixed in the present case, it would be advisable in future work to examine the model's performance with other comprehensive hyper-parameter tunings and sensitivity analysis. Besides, not only wave data as input, but also the integration of meteorological data such as wind and air pressure could be provided as additional input data to obtain a more consolidated deep-learning model framework.

4 Summary and Conclusions

In the present study, the hindcasting of extreme sea waves due to a cyclone was conducted by numerical modelling, and the near-real-time wave forecasting was carried out by deep-learning approach. Firstly, a top-down numerical simulation approach using the Weather Research and Forecasting (WRF) and Simulating WAves Nearshore (SWAN) models was applied to study the meteorological development and offshore wave characteristics due to cyclone Nargis near the coast of Myanmar. The WRF simulation results agree well with the observed data (in terms of the cyclone's track and minimum central pressure) from the India Meteorological Department. SWAN simulation results were compared with the WaveWatch 3 model by National Oceanic and Atmospheric Administration and also validated against available measurement data from satellites. Moreover, the model results show relatively good agreement with satellite measured wave data (significant wave height only), which shows a correlation coefficient value of 0.89. The SWAN and satellite comparisons also show better fit for high wave conditions than low waves, which is a driving factor for design and planning of coastal structures and coastal protection. The simulated maximum significant wave height of 7.3 m by SWAN is considerably higher in energy than the seasonal waves normally prevalent at Myanmar's deltaic coast, where low energy waves are dominant.

The possibility of high energy waves due to cyclones should be considered during the design and operation of coastal and offshore projects in the area, particularly given the risks that climate change can intensify cyclones in the future. Since Myanmar lacks a dense network of in-situ wave observational stations, the methodology used in the present thesis can potentially be applied to various numerical techniques for hindcasting and forecasting of wave characteristics. Moreover, since wave products derived from various oceanographic

satellites are available (with different reliability and accuracy levels), these satellite altimetry wave data, especially wave height, can be used as reference values to estimate the wave conditions for coastal areas in countries like Myanmar that have limited in-situ wave data network.

Secondly, wave condition (either low or high waves) forecasting was conducted by using artificial neural networks in an area that has an abundance of recorded data. To do so, a supervised deep-learning approach that employed the multi-layered Long Short Term Memory (LSTM) network, which can process the information in a sequential data set (time-series wave data), was used. The model was applied at Tottori and Kashima along the Japanese coast, where long-term wave records is available. The model was run to forecast the next 24 h of wave conditions (high or low) based on the previous 24 h, 48 h and 72 h wave data. The results show that the overall average waves classification accuracy of the model ranges from around 75 % to 99 % (with accuracies above 98% if at least three years of data are used to train the model). The application of deep-learning approach thus appears to outperform the traditional probabilistic approach and numerical wave models, and can be used as an advanced tool to assist the planning of possible working days at offshore construction sites.

To summarize, the present research applied two distinct wave prediction approaches: numerical modelling for extreme cyclonic waves prediction and deep-learning for near-real-time conditional wave forecasting. Each methodology highlights the different potential usage and applications of available measured wave data (ranging from satellite altimetry wave products and in-situ wave stations). The results suggest that satellite data can reflect the general wave climate information of a region which lacks a dense-network of in-situ wave observations. Similarly, the availability of long-term wave records is useful for advanced prediction technique, such as data mining with neural networks. Based on the current study, it

can be concluded that the numerical modelling technique is essentially applicable for exceptional extreme wave conditions, while the cutting-edge deep learning approach can be more effective for seasonal wave prediction to conduct real-time operational planning at coastal areas.

The present work considered the satellite recorded H_s only for the case of extreme waves due to a cyclone. In future work, it is recommended that a correlation analysis between the seasonal simulated wave parameters (available from open data sources such as NOAA) and satellite measured waves in the vicinity of Myanmar coast should be conducted, especially during the monsoon season (when high energy waves can take place). This could help to identify the seasonal anomalies in wave characteristics and improve planning work for the coastal regions of Myanmar. In addition, the present deep-learning model was applied only at two locations (Tottori and Kashima), and further verification of the model at additional locations along the Japan coast is recommended to analyse its performance at a variety of regions with different bathymetric and wave climate characteristics. The integration of additional input datasets in addition to wave data, such as wind and air pressure data, is also recommended to obtain a more comprehensive forecasting framework that further improves the accuracy of the model.

5 References

Baker D. B., Kyaw T., & Chua R. (2008). Post-Nargis Joint Assessment. The Tripartite Core Group of the Government of the Union of Myanmar, the Association of Southeast Asian Nations and the United Nations. https://www.recoveryplatform.org/assets/publication/Post-Nargis_Joint_Assessment.pdf. Accessed 8 Aug 2019

Battjes, J. A., & Janssen, J. P. F. M. (1978). Energy loss and set-up due to breaking of random waves. In Coastal engineering 1978 (pp. 569-587). http://resolver.tudelft.nl/uuid:2fba43fe-f8bd-42ac-85ee-848312d2e27e. Accessed 10 Aug 2019

Bhaskaran, P. K., Nayak, S., Bonthu, S. R., Murty, P. N., & Sen, D. (2013). Performance and validation of a coupled parallel ADCIRC–SWAN model for THANE cyclone in the Bay of Bengal. Environmental Fluid Mechanics, 13(6), 601-623. https://doi.org/10.1007/s10652-013-9284-5

Booij, N. R., Ris, R. C., & Holthuijsen, L. H. (1996). The "SWAN" wave model for shallow water, Proceedings of 25th International Conference on Coastal Engineering, pp. 668-676.

Booij, N. R., Ris, R. C., & Holthuijsen, L. H. (1999). A third ‐ generation wave model for coastal regions: 1. Model description and validation. Journal of geophysical research: Oceans, 104(C4), 7649-7666. https://doi.org/10.1029/98JC02622

Brezak, D., Bacek, T., Majetic, D., Kasac, J., & Novakovic, B. (2012, March). A comparison of feed-forward and recurrent neural networks in time series forecasting. In 2012 IEEE

Conference on Computational Intelligence for Financial Engineering & Economics (CIFEr) (pp. 1-6). IEEE.

Center for Excellence in Disaster Management and Humanitarian Assistance (CFE-DM) (2017). Myanmar (Burma) Disaster Management Reference Handbook. U.S. Department of Defense. https://www.cfe-dmha.org/LinkClick.aspx?fileticket=zf5i3c7xwDA%3D&portalid=0. Accessed 10 Aug 2019

Challenor, P. G., & Srokosz, M. A. (1991). Wave studies with the radar altimeter. International Journal of Remote Sensing, 12(8), 1671-1686. https://doi.org/10.1080/01431169108955200

Chen, C., Zhu, J., Lin, M., Zhao, Y., Wang, H., & Wang, J. (2017). Validation of the significant wave height product of HY-2 altimeter. Remote Sensing, 9(10), 1016. https://doi:10.3390/rs9101016

Deo, M. C., & Naidu, C.S. (1998). Real time wave forecasting using neural networks. Ocean engineering, 26(3), pp.191-203.

DeVries, P. M., Thompson, T. B., & Meade, B. J. (2017). Enabling large-scale viscoelastic calculations via neural network acceleration. Geophysical Research Letters, 44(6), 2662-2669.

Eldeberky, Y. (1996). Nonlinear transformation of wave spectra in the nearshore zone. Ph.D. thesis, Delft University of Technology, Department of Civil Engineering, The Netherlands. http://resolver.tudelft.nl/uuid:707ca57d-81c3-4103-bc6e-aae1c90fce63. Accessed 5 Aug 2019

Emanuel, K. (2005). Increasing destructiveness of tropical cyclones over the past 30 years. Nature, 436(7051), 686-688. https://doi.org/10.1038/nature03906

Esteban, M., Valenzuela, V. P., Yun, N. Y., Mikami, T., Shibayama, T., Matsumaru, R., ... & Nakamura, R. (2015). Typhoon Haiyan 2013 evacuation preparations and awareness. International Journal of Sustainable Future for Human Security, 3(1), 37-45. https://doi.org/10.24910/jsustain/3.1/3745

Farquhar, C. R., Deighton, H., Busswell, G., Snaith, H. M., Ash, E., Collard, F., ... & Pinnock, S. (2013). Globwave: A Global wave data portal. https://www.eumetsat.int/website/wcm/idc/idcplg?IdcService=GET_FILE&dDocName=PDF_CONF_P61_S6_02_DEIGHTON_V&RevisionSelectionMethod=LatestReleased&Rendition=Web. Accessed on 10 Aug 2019

Fosu, B. O., & Wang, S. Y. S. (2015). Bay of Bengal: coupling of pre-monsoon tropical cyclones with the monsoon onset in Myanmar. Climate Dynamics, 45(3), 697-709. https://doi.org/10.1007/s00382-014-2289-z

GEBCO Compilation Group (2020). GEBCO 2020 Grid. https://doi:10.5285/a29c5465-b138-234d-e053-6c86abc040b9

General Bathymetric Chart of the Oceans (GEBCO) (2020). Gridded bathymetry data. https ://www.gebco.net/data_and_produ cts/gridd ed_bathy metry data/

Girosi, F., Jones, M., & Poggio, T. (1995). Regularization theory and neural networks architectures. Neural computation, 7(2), pp.219-269.

Goodfellow, I., Bengio, Y., Courville, A., & Bengio, Y. (2016). Deep learning (Vol. 1, No. 2). Cambridge: MIT press.

Group, T. W. (1988). The WAM model—A third generation ocean wave prediction model. Journal of Physical Oceanography, 18(12), 1775-1810.

Hasselmann, K. F., Barnett, T. P., Bouws, E., Carlson, H., Cartwright, D. E., Eake, K., ... & Walden, H. (1973). Measurements of wind-wave growth and swell decay during the Joint North Sea Wave Project (JONSWAP). Ergaenzungsheft zur Deutschen Hydrographischen Zeitschrift, Reihe A. http://resolver.tudelft.nl/uuid:f204e188-13b9-49d8-a6dc-4fb7c20562fc. Accessed 12 Aug 2019

Hasselmann, S., Hasselmann, K., Allender, J., & Barnett, T. P. (1985). Computations and parameterizations of the nonlinear energy transfer in a gravity-wave specturm. Part II: Parameterizations of the nonlinear energy transfer for application in wave models. Journal of Physical Oceanography, 15(11), 1378-1391. https://doi.org/10.1175/1520-0485(1985)015<1378:CAPOTN>2.0.CO;2

Hithin, N. K., Kumar, V. S., & Shanas, P. R. (2015). Trends of wave height and period in the Central Arabian Sea from 1996 to 2012: a study based on satellite altimeter data. Ocean Engineering, 108, 416-425. https://doi.org/10.1016/j.oceaneng.2015.08.024

Hoarau, K., Bernard, J., & Chalonge, L. (2012). Intense tropical cyclone activities in the northern Indian Ocean. International Journal of Climatology, 32(13), 1935-1945. https://doi.org/10.1002/joc.2406

Hochreiter, S., & Schmidhuber, J. (1997). Long short-term memory. Neural computation, 9(8), 1735-1780. https://doi:10.1162/neco.1997.9.8.1735

Hong, S. Y., & Lim, J. O. J. (2006). The WRF single-moment 6-class microphysics scheme (WSM6). Asia-Pacific Journal of Atmospheric Sciences, 42(2), 129-151.

http://www2.mmm.ucar.edu/wrf/users/phys_refs/MICRO_PHYS/WSM6.pdf. Accessed 8 Aug 2019

Hong, S. Y., Noh, Y., & Dudhia, J. (2006). A new vertical diffusion package with an explicit treatment of entrainment processes. Monthly weather review, 134(9), 2318-2341. https://doi.org/10.1175/MWR3199.1

Iacono, M. J., Delamere, J. S., Mlawer, E. J., Shephard, M. W., Clough, S. A., & Collins, W. D. (2008). Radiative forcing by long‐lived greenhouse gases: Calculations with the AER radiative transfer models. Journal of Geophysical Research: Atmospheres, 113(D13). https://doi.org/10.1029/2008JD009944

Islam, T., Srivastava, P. K., Rico-Ramirez, M. A., Dai, Q., Gupta, M., & Singh, S. K. (2015). Tracking a tropical cyclone through WRF–ARW simulation and sensitivity of model physics. Natural Hazards, 76(3), 1473-1495. https://doi.org/10.1007/s11069-014-1494-8

James, S. C., Zhang, Y., & O'Donncha, F. (2018). A machine learning framework to forecast wave conditions. Coastal Engineering, 137, 1-10. https://doi:10.1016/j.coastaleng.2018.03.004

Japan International Cooperation Agency (JICA) (2015). Coungry Report Myanmar: Natural Disaster Risk Assessment and Area Business Continuity Plan Formulation for Industrial Agglomerated Areas in the ASEAN Region. http://open_jicareport.jica.go.jp/pdf/1000023395.pdf. Accessed 8 Aug 2019

Juba, B., & Le, H. S. (2019, July). Precision-recall versus accuracy and the role of large data sets. In Proceedings of the AAAI Conference on Artificial Intelligence (Vol. 33, No. 01, pp. 4039-4048).

Kain, J. S. (2004). The Kain–Fritsch convective parameterization: an update. Journal of applied meteorology, 43(1), 170-181. https://doi.org/10.1175/1520-0450(2004)043%3C0170:TKCPAU%3E2.0.CO;2

Kim, S., Matsumi, Y., Pan, S., & Mase, H. (2016). A real-time forecast model using artificial neural network for after-runner storm surges on the Tottori coast, Japan. Ocean Engineering, 122, 44-53. https://doi:10.1016/j.oceaneng.2016.06.017

Knutson, T. R., McBride, J. L., Chan, J., Emanuel, K., Holland, G., Landsea, C., ... & Sugi, M. (2010). Tropical cyclones and climate change. Nature geoscience, 3(3), 157-163. https://doi.org/10.1038/ngeo779

Komen, G. J., Hasselmann, S., & Hasselmann, K. (1984). On the existence of a fully developed wind-sea spectrum. Journal of physical oceanography, 14(8), 1271-1285. https://doi.org/10.1175/1520-0485(1984)014<1271:OTEOAF>2.0.CO;2

Savitha, R., & Al Mamun, A. (2017). Regional ocean wave height prediction using sequential learning neural networks. Ocean Engineering, 129, 605-612. https://doi:10.1016/j.oceaneng.2016.10.033

Kumar, N. K., Savitha, R., & Al Mamun, A. (2018). Ocean wave height prediction using ensemble of extreme learning machine. Neurocomputing, 277, 12-20. https://doi:10.1016/j.neucom.2017.03.092

Kyaw, T. O., & Shibayama, T. (2018). Numerical Simulation of Cyclone Nargis (2008) and Its Related Wave Field at Myanmar Coast by Using WRF-SWAN Model. Coastal Engineering Proceedings, 1, 36. https://doi.org/10.9753/icce.v36.waves.16

LeCun, Y., Bengio, Y., Hinton, G. (2015). Deep learning. Nature 521, 436–444.

Leelawat, N., Mateo, C. M. R., Gaspay, S. M., Suppasri, A., & Imamura, F. (2014). Filipinos' views on the disaster information for the 2013 Super Typhoon Haiyan in the Philippines. Int J Sustain Future Hum Secur, 2(2), 61-73. https://doi.org/10.24910/jsustain/2.2/1628

Li, W. W., Wang, C., Wang, D., Yang, L., & Deng, Y. (2012). Modulation of low-latitude west wind on abnormal track and intensity of tropical cyclone Nargis (2008) in the Bay of Bengal. Advances in Atmospheric Sciences, 29(2), 407-421. https://doi.org/10.1007/s00376-011-0229-y

Lin, I. I., Chen, C. H., Pun, I. F., Liu, W. T., & Wu, C. C. (2009). Warm ocean anomaly, air sea fluxes, and the rapid intensification of tropical cyclone Nargis (2008). Geophysical Research Letters, 36(3). https://doi.org/10.1029/2008GL035815

Londhe, S. N., Shah, S., Dixit, P. R., Nair, T. B., Sirisha, P., & Jain, R. (2016). A coupled numerical and artificial neural network model for improving location specific wave forecast. Applied Ocean Research, 59, 483-491. https://doi:10.1016/j.apor.2016.07.004

Mandal, S., & Prabaharan, N. (2010). Ocean wave prediction using numerical and neural network models. The Open Ocean Engineering Journal, 3(1). https://doi:10.2174/1874835X01003010012

Myanmar Information Management Unit (MIMU) (2019). Population in low-lying coastal zone.https://themimu.info/sites/themimu.info/files/documents/Population_Map_Population_in_Low-Lying_Coastal_Area_MIMU1646v01_23May2019_A4_0.pdf. Accessed on 12 Oct 2020

Myanma Port Authority (MPA) (2020). Ports and Terminals Data Information. http://www.mpa.gov.mm/facts-figures/facts-international-terminals-yangon-port-0. Accessed on 20 Oct 2020

Nagai, T. (2000). Infragravity wave observation around Japan by the Nationwide Ocean Wave information network for Ports and HArbourS (NOWPHAS). In Proc. Fourth Int. Conf. Hydrodynam.(ICHD'2000) (pp. 509-514).

Nakamura, R., Shibayama, T., Esteban, M., & Iwamoto, T. (2016). Future typhoon and storm surges under different global warming scenarios: case study of typhoon Haiyan (2013). Natural Hazards, 82(3), 1645-1681. https://doi.org/10.1007/s11069-016-2259-3

National Centre for Atmospheric Research (NCAR) (2017). Weather Reseach and Forecasting-ARW. Version3 Modeling System User's Guide. http://www2.mmm.ucar.edu/wrf/users/docs/user_guide_V3.8/ARWUsersGuideV3.8.pdf. Accessed 9 Aug 2019

Nayak, S., Bhaskaran, P. K., & Venkatesan, R. (2012). Near-shore wave induced setup along Kalpakkam coast during an extreme cyclone event in the Bay of Bengal. Ocean Engineering, 55, 52-61. https://doi.org/10.1016/j.oceaneng.2012.07.036

Nishizaki, S., Shibayama, T., Takabatake, T., & Nakamura, R. (2018). Hindcasting of wave climate along the Pacific Coast of Japan in october 2014. In ASIAN AND PACIFIC COASTS 2017: Proceedings of the 9th International Conference on APAC 2017 (pp. 129-138). https://doi.org/10.1142/9789813233812_0013

O'Donncha, F., Zhang, Y., Chen, B., & James, S. C. (2018). An integrated framework that combines machine learning and numerical models to improve wave-condition forecasts. Journal of Marine Systems, 186, 29-36. https://doi:10.1016/j.jmarsys.2018.05.006

Pattanaik, D. R., & Rao, Y. R. (2009). Track prediction of very severe cyclone 'Nargis' using high resolution weather research forecasting (WRF) model. Journal of earth system science, 118(4), 309-329. https://doi.org/10.1007/s12040-009-0031-8

Peng, G. (2014). What is the difference between FNL and GFS. National Center for Atmospheric Research. https://rda.ucar.edu/datasets/ds083.2/docs/FNLvGFS.pdf. Accessed 5 Aug 2019

Prahlada, R., & Deka, P. C. (2015). Forecasting of time series significant wave height using wavelet decomposed neural network. Aquatic Procedia, 4, 540-547. https://doi:10.1016/j.aqpro.2015.02.070

Raju, P. V. S., Potty, J., & Mohanty, U. C. (2011). Sensitivity of physical parameterizations on prediction of tropical cyclone Nargis over the Bay of Bengal using WRF model. Meteorology and Atmospheric Physics, 113(3), 125-137. https://doi.org/10.1007/s00703-011-0151-y

Raschka, S., & Mirjalili, V. (2017). Python Machine Learning: Machine Learning and Deep Learning with Python. Scikit-Learn, and TensorFlow. Second edition ed.

Raschka, S., Mirajalili, V. (2019). Python machine learning. Packt Publishing.

Ribal, A., & Young, I. R. (2019). 33 years of globally calibrated wave height and wind speed data based on altimeter observations. Scientific data, 6(1), 1-15. https://doi.org/10.1109/TGRS.2009.2020793

Roca, M., Laxon, S., & Zelli, C. (2009). The EnviSat RA-2 instrument design and tracking performance. IEEE Transactions on Geoscience and Remote Sensing, 47(10), 3489-3506.

Rogers, E., Black, T., Ferrier, B, et. Al. (2001). Changes to the NCEP Meso Eta Analysis and Forecast System: Increase in resolution, new cloud microphysics, modified precipitation assimilation, modified 3DVAR analysis. National Weather Service Technical Procedures Bulletin 488:15. https://www.emc.ncep.noaa.gov/mmb/mmbpll/. Accessed 3 Aug 2019

Saito, K., Kuroda, T., Kunii, M., & Kohno, N. (2010). Numerical simulation of Myanmar cyclone Nargis and the associated storm surge part II: ensemble prediction. Journal of the Meteorological Society of Japan. Ser. II, 88(3), 547-570. https://doi.org/10.2151/jmsj.2010-316

Samiksha, S. V., Polnikov, V. G., Vethamony, P., Rashmi, R., Pogarskii, F., & Sudheesh, K. (2015). Verification of model wave heights with long-term moored buoy data: Application to wave field over the Indian Ocean. Ocean Engineering, 104, 469-479. https://doi.org/10.1016/j.oceaneng.2015.05.020

Schmidhuber, J. (2015). Deep learning in neural networks: an overview. Neural Network. 61, 85–117.

Shibayama, T., Aoki, Y., & Takagi, H. (2010). Field survey and analysis of flood behavior of storm surge due to cyclone Nargis in Myanmar. Annual Journal of Civil Engineering in the Ocean, JSCE, 26, 429-434. (in Japanese)

Shibayama, T., Takagi, H., & Hnu, N. (2010). Disaster survey after the cyclone Nargis in 2008. In Asian and Pacific Coasts 2009: (In 4 Volumes, with CD-ROM) (pp. 190-193). https://doi.org/10.1142/9789814287951_0069

Shimura, T, Mori, N (2019) High-resolution wave climate hindcast around Japan and its spectral representation. *Coastal Engineering*, Vol.151, pp.1–9.

Shrivastava, R., & Krishna, T. C. (2018). Correlation Enhanced Machine Learning Approach Based Wave Height Prediction. International Journal Online of Science 4 (5 May): 1–10. http://ijoscience.com/ojsscience/index.php/ojsscience/article/view/136

Singh, O. P., Khan, T. M. A., & Rahman, M. S. (2001). Has the frequency of intense tropical cyclones increased in the north Indian Ocean?. Current science, 575-580.

Skamarock, W. C., Klemp, J. B., Dudhia, J., Gill, D. O., Barker, D. M., Wang, W., & Powers, J. G. (2008). A description of the Advanced Research WRF version 3. NCAR Technical note-475+ STR. https://doi.org/10.5065/D68S4MVH

Srinivas, D., & Rao, D. V. B. (2014). Implications of vortex initialization and model spin-up in tropical cyclone prediction using Advanced Research Weather Research and Forecasting Model. Natural hazards, 73(2), 1043-1062. https://doi.org/10.1007/s11069-014-1125-4

Srivastava, N., Hinton, G., Krizhevsky, A., Sutskever, I., & Salakhutdinov, R. (2014). Dropout: a simple way to prevent neural networks from overfitting. The journal of machine learning research, 15(1), 1929-1958.Sverdrup, H. U., & Munk, W. H. (1947). Wind, sea and swell: Theory of relations for forecasting (No. 303). Hydrographic Office.

SWAMP Group (1985). Ocean wave modeling. Springer Science & Business Media.

SWAN (2009). SWAN User Manual (SWAN Cycle III version 41.31). Delft University of Technology, The Netherlands. http://swanmodel.sourceforge.net/download/zip/swanuse.pdf. Accessed 30 July 2019

Tasnim, K. M., Esteban, M., & Shibayama, T. (2015). Observations and Numerical Simulation of Storm Surge due to Cyclone Sidr 2007 in Bangladesh. In Handbook of Coastal Disaster Mitigation for Engineers and Planners (pp. 35-53). Butterworth-Heinemann. https://doi.org/10.1016/B978-0-12-801060-0.00003-4

Tasnim, K. M., Shibayama, T., Esteban, M., Takagi, H., Ohira, K., & Nakamura, R. (2015). Field observation and numerical simulation of past and future storm surges in the Bay of Bengal: case study of cyclone Nargis. Natural Hazards, 75(2), 1619-1647. https://doi.org/10.1007/s11069-014-1387-x

Mukul Tewari, N. C. A. R., Tewari, M., Chen, F., Wang, W., Dudhia, J., LeMone, M., ... & Cuenca, R. H. (2004, January). Implementation and verification of the unified NOAH land surface model in the WRF model (Formerly Paper Number 17.5). In 20th conference on weather analysis and forecasting/16th conference on numerical weather prediction (pp. 11-15). https://opensky.ucar.edu/islandora/object/conference:1576. Accessed 12 Aug 2019

Tolman, H.L. (2002). Testing of WAVEWATCH III version 2.22 in NCEP's NWW3 ocean wave model suite, Tech Note 214, NOAA/NWS/NCEP/OMB, 99p.

Tolman, H. L., Krasnopolsky, V. M., & Chalikov, D. V. (2005). Neural network approximations for nonlinear interactions in wind wave spectra: direct mapping for wind seas in deep water. Ocean Modelling, 8(3), 253-278.

Tom, T. H., Ikemoto, A., Mase, H., Kawasaki, K., Takeda, M., & Kim, S. (2019). Wave Prediction in the Sea of Japan by Deep Learning Using Meteorological Data. Journal of Japan Society of Civil Engineers, Ser. B2 (Coastal Engineering), 75(2), I_145-I_150.

Tsuboki, K. (2008). High-resolution simulations of high-impact weather systems using the cloud-resolving model on the Earth Simulator. In High Resolution Numerical Modelling of the Atmosphere and Ocean (pp. 141-156). Springer, New York, NY. https://doi.org/10.1007/978-0-387-49791-4_9

United Nations Environment Programme (UNEP) (2009). Learning from Cyclone Nargis: Investing in the Environment for Livelihoods and Disaster Risk Reduction: A Case Study.https://wedocs.unep.org/bitstream/handle/20.500.11822/14116/myanmar_cyclone nargis_case_study.pdf?sequence=1&isAllowed=y. Accessed on 20 Oct 2020

Vishnu, S., Francis, P. A., Shenoi, S. S. C., & Ramakrishna, S. S. V. S. (2016). On the decreasing trend of the number of monsoon depressions in the Bay of Bengal. Environmental Research Letters, 11(1), 014011. https://doi.org/10.1088/1748-9326/11/1/014011

Wang, S. Y., Buckley, B. M., Yoon, J. H., & Fosu, B. (2013). Intensification of premonsoon tropical cyclones in the Bay of Bengal and its impacts on Myanmar. Journal of Geophysical Research: Atmospheres, 118(10), 4373-4384. https://doi.org/10.1002/jgrd.50396

Woo, H. J., & Park, K. A. (2017). Long-term trend of satellite-observed significant wave height and impact on ecosystem in the East/Japan Sea. Deep Sea Research Part II: Topical Studies in Oceanography, 143, 1-14. https://doi.org/10.1016/j.dsr2.2016.09.003

World Meteorological Organization (WMO) (2018). Observing Systems Capability Analysis and Review Tool: List of all Satellites. https://www.wmo-sat.info/oscar/satellites. Accessed 3 July 2019

Yoon, J. H., & Huang, W. R. (2012). Indian monsoon depression: Climatology and variability. Modern climatology, 13, 45-72. https://doi.org/10.5772/37917

Zaremba, W., Sutskever, I., & Vinyals, O. (2014). Recurrent neural network regularization. arXiv preprint arXiv:1409.2329.

Appendix A

Layer (type)	Output Shape	Param #
lstm_15 (LSTM)	(None, 12, 128)	67072
lstm_16 (LSTM)	(None, 12, 128)	131584
flatten_8 (Flatten)	(None, 1536)	0
dropout_8 (Dropout)	(None, 1536)	0
dense_22 (Dense)	(None, 128)	196736
dense_23 (Dense)	(None, 128)	16512
dense_24 (Dense)	(None, 2)	258

Total params: 412,162
Trainable params: 412,162
Non-trainable params: 0

Figure A1. Configuration of hidden layers of the developed deep-learning wave forecasting model for 24 h preceding time

Layer (type)	Output Shape	Param #
lstm_7 (LSTM)	(None, 24, 128)	67072
lstm_8 (LSTM)	(None, 24, 128)	131584
flatten_4 (Flatten)	(None, 3072)	0
dropout_4 (Dropout)	(None, 3072)	0
dense_10 (Dense)	(None, 128)	393344
dense_11 (Dense)	(None, 128)	16512
dense_12 (Dense)	(None, 2)	258

Total params: 608,770
Trainable params: 608,770
Non-trainable params: 0

Figure A2. Configuration of hidden layers of the developed deep-learning wave forecasting model for 48 h preceding time

Layer (type)	Output Shape	Param #
lstm_33 (LSTM)	(None, 36, 128)	67072
lstm_34 (LSTM)	(None, 36, 128)	131584
flatten_17 (Flatten)	(None, 4608)	0
dropout_17 (Dropout)	(None, 4608)	0
dense_49 (Dense)	(None, 128)	589952
dense_50 (Dense)	(None, 128)	16512
dense_51 (Dense)	(None, 2)	258

Total params: 805,378
Trainable params: 805,378
Non-trainable params: 0

Figure A3. Configuration of hidden layers of the developed deep-learning wave forecasting model for 72 h preceding time

List of Research Achievements

(a) Journals

Kyaw T.O., Esteban M., Mäll M., Shibayama T. (2021). Extreme waves induced by cyclone Nargis at Myanmar coast: Numerical modeling vs. satellite observations. Natural Hazards, 106(3), 1797-1818.

Harnantyari A.S., Takabatake T., Esteban M., Valenzuela P., Nishida Y., Shibayama T., Achiari H., Marzuki A.G., Marzuki M.F.H., Aránguiz R. and **Kyaw T.O.** (2020). Tsunami awareness and evacuation behaviour during the 2018 Sulawesi Earthquake tsunami. International journal of disaster risk reduction, 43, p.101389.

Takabatake T., Mäll M., Esteban M., Nakamura R., **Kyaw T.O.,** Ishii H., Valdez J.J., Nishida Y., Noya F. and Shibayama T. (2018). Field survey of 2018 Typhoon Jebi in Japan: lessons for disaster risk management. Geosciences, 8(11), p.412.

Takabatake T., Shibayama T., Esteban M., Achiari H., Nurisman N., Gelfi M., Tarigan T.A., Kencana E.R., Fauzi M.A.R., Panalaran S., Harnantyari A.S and **Kyaw T. O.** (2019). Field survey and evacuation behaviour during the 2018 Sunda Strait tsunami. Coastal Engineering Journal, 61(4), 423-443.

(b) Conferences

Kyaw T. O., Shibayama T. Numerical simulation of cyclone Nargis (2008) and its related wave field at Myanmar coast by using WRF-SWAN model. The 36th International Conference on Coastal Engineering. Baltimore, US, July 30 - August 3, 2018. (peer reviewed, presentation type: oral)

Kyaw T. O., Shibayama T., Shibutani Y., Kotake Y. Development of a deep-learning based wave forecasting model using LSTM network. Virtual International Conference on Coastal Engineering. 6‐9 October 2020. (peer reviewed, presentation type: oral)

Kyaw T. O., Shibayama T., Shibutani Y., Kotake Y. Wave forecasting at Japan coast: an advanced deep learning approach. The 10th International Conference on Coastal and Port Engineering in Developing Countries. Manila, Philippines. (postponed to late 2021)

稲垣直人, 柴山知也, 高畠知行, Miguel Esteban, Martin Maell, **Thit Oo Kyaw**. 突風による水塊輸送と越波流量に与える影響. 第 33 回日本沿岸域学会研究討論会, 長崎県勤労福祉会館. (2021 年 6 月へ延期).

馬渡竜輝, 高畠知行, **Thit Oo Kyaw**, 柴山知也, 澁谷容子, 小竹康夫. 深層学習を用いた波浪予測手法の開発と日本沿岸域への適用性. 第 28 回海洋工学シンポジウム, 日本大学理工学部.